RESEARCH REPORT VTT-R-00028-25

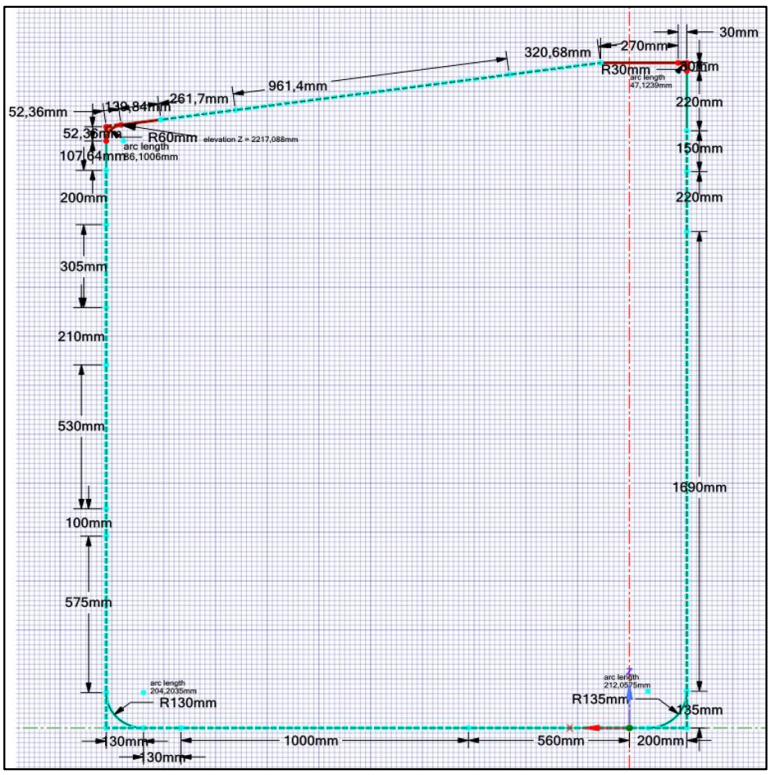

Analysis of APSARA Test Facility Data with Apros and CATHARE-3 Codes – 2 (Two Phase Cases)

Author: Fares Alblouwy

Contributors (IRSN, G-MET): Christophe Herer, Sebastien Desmarest, Pierre Ruyer, Adam Trabelsi, Amina Younsi, and Paulin Ferro

Confidentiality: VTT Public

Report's title Analysis of APSARA Test Facility Data with Apros and CATHARE-3 Codes – 2 (Two Phase Cases)	
Customer, contact person, address SAFER2028, Eero Virtanen, STUK	**Order reference** SAFER 15/2024
Project name Analysis of Passive Safety Systems' Operations and Modelling	**Project number/Short name** 137928/ESPO
Author(s) Fares Alblouwy	**Pages** 38
Keywords Apros,CATHARE,APSARA,Natural Circulation,Two-phase	**Report identification code** VTT-R-00028-25

Summary

Short-listed two-phase test cases conducted at the APSARA facility were simulated using Apros code (version 6.13.04) by the VTT team and CATHARE code (C-3) by the IRSN team. This work aims to study natural circulation phenomena, evaluate the capabilities of the codes in simulating this critical safety-related behaviour in nuclear power plants, and support pre-calculation efforts for the development of the ALCINA facility, a test loop designed by IRSN to investigate natural circulation phenomena.

Initially, the publicly available APSARA data were verified and analysed. Necessary assumptions were made to refine the scope of the simulation analysis. While power, pressure, and the heater's inlet temperature were user-controlled parameters, the simulations and experiments primarily focused on determining the flow rate, outlet temperature, and void generation within the loop.

For single-phase simulations, previously published in the report *"Analysis of APSARA Test Facility Data with Apros and CATHARE-3 Codes"*, both codes demonstrated acceptable accuracy in estimating mass flow rates. However, the calculated values were underestimated by less than 4 %. This discrepancy was attributed to assumptions made due to limited data availability and the exclusion of heat loss effects during simulations.

In the present report, which focuses on two-phase cases, the deviations are more significant. These higher deviations are linked to uncertainties caused by modifications to the facility geometry during modelling, necessitated by gaps in the available data. Consequently, the increased uncertainty in the geometrical modelling prevents the use of these studies for validation purposes.

Despite these challenges, the simulation exercise achieved its objectives. Using a benchmarking approach, it successfully highlighted key aspects of natural circulation behaviour and the related simulation features of both codes. Furthermore, this work provides valuable insights to support pre-calculation activities for the ALCINA facility.

Confidentiality	VTT Public

Espoo 30.1.2025

Written by	**Reviewed by**
Fares Alblouwy, Research Scientist and Project Manager	Seppo Hillberg, Senior Scientist

VTT's contact address
VTT Technical Research Centre of Finland Ltd, P.O. Box 1000, FI-02044 VTT, Finland.

Distribution (customer and VTT)
by email to SAFER2028 Technical Advisory Group 2.1 (TAG).

Approval

VTT TECHNICAL RESEARCH CENTRE OF FINLAND LTD

Date:	
Signature:	
Name:	Joona Kurki
Title:	Research Team Leader

Preface

The ESPO (Analysis of Passive Safety Systems' Operations and Modelling) project, supported by the Finnish Research Programme on Nuclear Power Plant Safety 2023 - 2025 (SAFER2028), focuses on exploring the behaviour of passive safety systems and improving computational analysis techniques. The research relies on data produced by experimental facilities participating in ongoing projects under the OECD/NEA (Organisation for Economic Co-operation and Development / Nuclear Energy Agency) and involves collaboration with international partners, including the French IRSN (Institut de Radioprotection et de Sûreté Nucléaire).

The project aims to enhance the understanding of passive safety system operations, identifying scenarios that may pose challenges to current analysis methods. It seeks to overcome these challenges by developing and refining analysis models and tools. A key component of ESPO is fostering knowledge transfer through mentorship and collaboration between experienced researchers and their junior counterparts, ensuring continuous development of expertise in essential safety topics like natural circulation. Furthermore, the project is committed to maintaining and strengthening international research partnerships.

The outcomes presented in this report are the result of collaborative efforts among teams from VTT, IRSN, and G-MET. Special acknowledgment is extended to Christophe Herer, Sébastien Desmarest, Pierre Ruyer, Amina Younsi (all from IRSN), and Paulin Ferro (G-MET), whose work on the APSARA model, data verification, detailed discussions, and contributions of CATHARE-3 data, results, and descriptions have been invaluable in the development of this report.

Espoo 29.01.2025

Fares Alblouwy,
Project manager

Content

1. Introduction

This report conducts a benchmark analysis on experimental data featured in the publicly available report titled "Analysis of Experimental Data on Two-Phase Natural Circulation From the Flow Pattern Transition Instability Studies Facility at APSARA Reactor" [1]. The report analysis focuses on void fraction and mass flow rate variations under different natural circulation conditions, comparing the outcomes to diverse thermal-hydraulic models, including the homogeneous and drift flux model.

Leveraging the technical collaboration between the Technical Research Center of Finland (VTT) and the French Institute for Radiological Protection and Nuclear Safety (IRSN), this data is employed for a comprehensive benchmark analysis and code-to-code comparison. The objective is to deepen the understanding of natural circulation phenomena, a cornerstone of nuclear passive safety systems. Additionally, the analysis supports IRSN's pre-calculation efforts for constructing the natural circulation passive safety loop of the ALCINA facility (part of the Passive Systems Thermal hydraulic Investigations for Safety project (PASTIS[1])), evaluating the capabilities of the Apros and CATHARE 3 (C-3) thermal hydraulic codes through benchmarking and code-to-code comparison.

Given the outlined objective and scope, this analysis cannot be used for code validation purposes due to the significant uncertainties introduced into the model. These uncertainties arise from the lack of detailed geometrical information in the original reference report, which necessitated incorporating approximations into the simulation models. However, this analysis contributes to investigating simulation capabilities, numerical limitations, and uncertainties while also supporting the pre-calculation of the ALCINA facility.

In 2025, under the ESPO project framework, the focus will shift to addressing the open questions by examining the numerical methods implemented in Apros. The goal is to provide an overview of the limitations and challenges associated with simulating natural circulation in passive safety systems.

[1] This project benefits from a grant from the French government managed by the Agence Nationale de la Recherche under the title of France 2030 with the reference " ANR-22-PAST-0001 "

2. APSARA Experimental Facility

2.1 Description of the APSARA Facility

Constructed in 1956, APSARA stands as an Indian pool-type nuclear research reactor [2]. Within its reactor hall, a dedicated steam/liquid natural circulation loop was established to conduct experimental investigations into natural circulation phenomena under diverse boundary conditions. The experimental facility, depicted in Figure 1, was designed to explore flow pattern transition instability and is capable of operating at a maximum pressure of 70 bar and a temperature of 315 °C. Employing Neutron Radiography, this facility enables visual observation of flow patterns and void formation within the loop.
The test section features a directly electrically heated tubular segment with a maximum power capacity of 10 kW. The outlet of this test section is connected to the midpoint of the steam drum via a riser. Steam generated in the loop rises, through the steam drum, towards a condenser, and the resulting condensate is directed back to the steam drum. While the water level inside the steam drum is maintained above the mid-point, the buoyancy-driven flow originates from the density differences between the loop's hot and cold legs [1] [3].

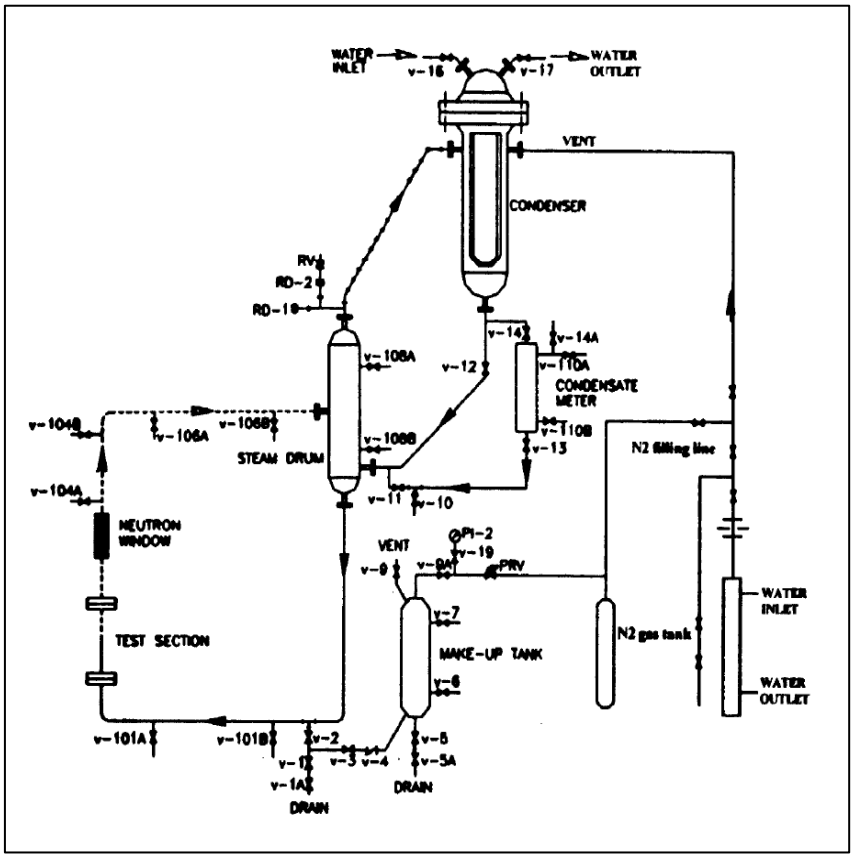

Figure 1: APSARA Experimental Facility

The facility is equipped with 1 mm diameter K-type thermocouples to measure temperatures at the heater inlet, outlet, and various locations. A pressure transducer inside the steam drum records the system's pressure. The steam drum is linked to a condenser where steam rises, condenses, and subsequently returns to the steam drum and back into the loop. The key features of the facility are summarized in Table 1.

Table 1: APSARA Test Facility Main Characteristics

Parameter	Value	Note
Inner Diameter [mm]	9.1	--
Outer Diameter [mm]	12.1	--
Heater Length [mm]	575	--
Steam drum Length [mm]	Not Known	See Section 2.2

2.2 Description of Simulation models

Considering the information provided by the reference report [1] and the absence of geometrical details for the remaining experimental facility, the simulation models will focus solely on replicating the test loop with certain assumed modifications to emulate the thermodynamic phenomena of the conducted experiments. These assumptions are derived and agreed upon between the two codes' users. It is highlighted that both models used in Apros and C-3 should be consistent to make proper comparison.
Geometrical details of the test loop, as depicted in Figure 2, are available, but insulations for the loop and other information regarding the upper part of the steam drum and condenser are not provided. The steam drum and condenser configuration were substituted with a modeled Heat Exchanger (HX) using a best-estimate technique to dissipate heat outside the system, mimicking the steam drum-condenser setup. The heat exchanger, a tube and shell type, has a length of 250 mm[2] (from the steam drum bottom to the mid-point), and the tube shares the same inner diameter as the test loop, i.e., 9.1 mm.

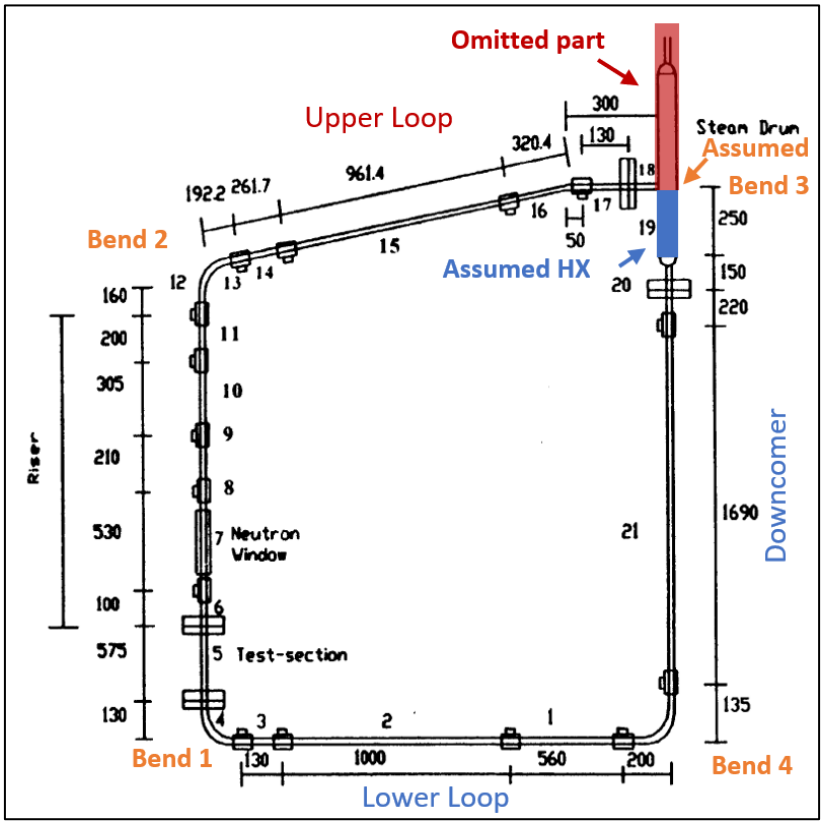

Figure 2: Dimensions of the Test Loop

[2] Two analysis rounds have been performed for Apros model with different HX lengths (250 and 400 mm), while C-3 data is provided based on HX of 400 mm length.

Figure 2 depicts the Isometric view (ISO) illustrating the loop dimensions [4]. Therefore, a design software (Ansys) was employed to precisely predict the dimensions of the loop bends. The subsequent figures present the geometrical details utilized in constructing the simulation models.

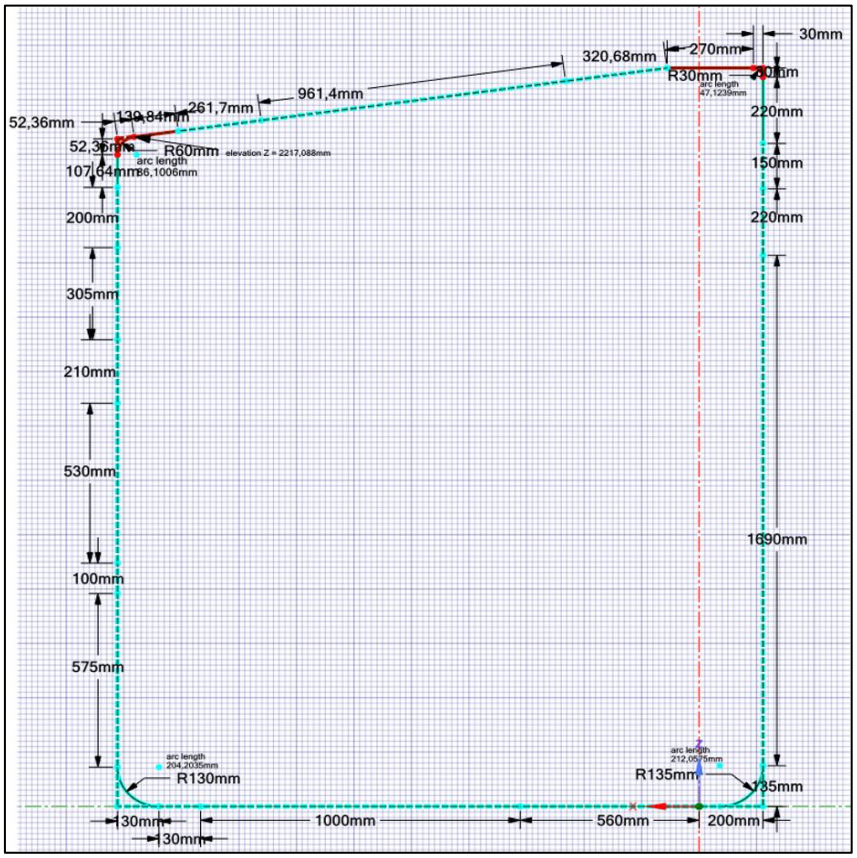

Figure 3: Geometrical Dimensions of Simulation Models

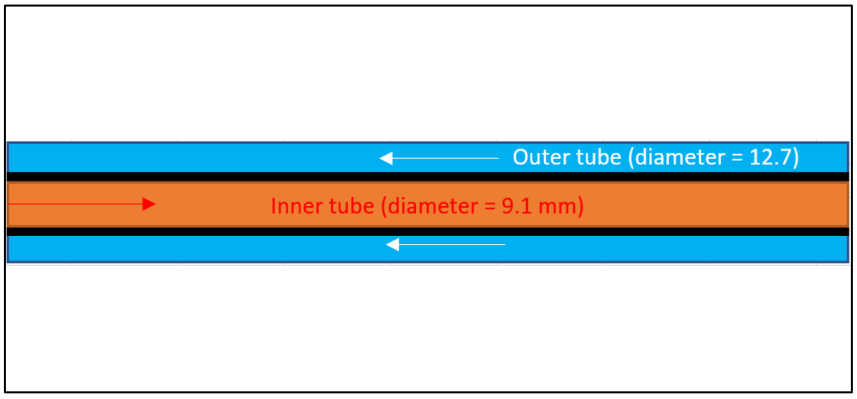

Figure 4: Configuration of Assumed Heat Exchanger

Considering Figure 3, the angle bends were assumed to be 90º, for bend 1,3, and 4 (lower left corner, upper right corner and lower right corner, respectively), while the angle for bend 2 is calculated to be 97.7°. The Form Loss coefficient of the bends is determined using the following Equation (1) [5]:

$$k = 0.9\sin(\alpha) * 0.21 * \left(\frac{Rc}{dh}\right)^{-0.25} \quad (1)$$

where:
α: *Bend angle.*
Rc: *Bend radius.*
dh: *Inner diameter.*

Table 2 illustrates the primary dimensions of the test loop employed in the simulation models.

Table 2: Test Loop Dimensions

Pipe #	Length (m)	OD (mm)	ID (mm)	SPL (-)	Height (m)	Elevation Before (m)	Elevation After (m)	Accumulated Length (m)
1	0.5600	12.7	9.1	0.00000	0.00000	0.00000	0.00000	0.56000
2	1.0000	12.7	9.1	0.00000	0.00000	0.00000	0.00000	1.56000
3	0.1300	12.7	9.1	0.00000	0.00000	0.00000	0.00000	1.69000
Bend 1	0.2042	12.7	9.1	0.09722	0.13000	0.00000	0.13000	1.89420
Test Section	0.5750	12.7	9.1	0.00000	0.57500	0.13000	0.70500	2.46920
6	0.1000	12.7	9.1	0.00000	0.10000	0.70500	0.80500	2.56920
Neutron Window	0.5300	12.7	9.1	0.00000	0.53000	0.80500	1.33500	3.09920
8	0.2100	12.7	9.1	0.00000	0.21000	1.33500	1.54500	3.30920
9	0.3050	12.7	9.1	0.00000	0.30500	1.54500	1.85000	3.61420
10	0.2000	12.7	9.1	0.00000	0.20000	1.85000	2.05000	3.81420
11	0.1076	12.7	9.1	0.00000	0.10760	2.05000	2.15764	3.92184
Bend 2	0.0861	12.7	9.1	0.11686	0.05945	2.15764	2.21709	4.00794
13	0.1398	12.7	9.1	0.00000	0.01893	2.21709	2.23602	4.14778
14	0.2617	12.7	9.1	0.00000	0.03543	2.23602	2.27144	4.40948
15	0.9614	12.7	9.1	0.00000	0.13014	2.27144	2.40159	5.37088
16	0.3207	12.7	9.1	0.00000	0.04341	2.40159	2.44500	5.69156
17	0.2700	12.7	9.1	0.00000	0.00000	2.44500	2.44500	5.96156
Bend 3	0.0471	12.7	9.1	0.14026	0.03000	2.44500	2.41500	6.00869
HX	0.2500	12.7	9.1	0.00000	0.25000	2.41500	2.16500	6.25869
20	0.3400	12.7	9.1	0.00000	0.34000	2.16500	1.82500	6.59869
21	1.6900	12.7	9.1	0.00000	1.69000	1.82500	0.13500	8.28869
Bend 4	0.2121	12.7	9.1	0.09630	0.13500	0.13500	0.00000	8.50075
22	0.0650	12.7	9.1	0.00000	0.00000	0.00000	0.00000	8.56575
Total								**8.56575**

2.3 Experimental Data Processing and Verification

To ease the integration of experimental data, the tabulated information in the primary report [1] was initially extracted into an editable format using Optical Character Recognition (OCR) software. Subsequently, a thorough verification process ensured the accurate replication of numerical values.
While scrutinizing the data, certain discrepancies emerged. For instance, in some cases, voids were observed inside the tube, even though temperature and pressure readings indicated a sub-cooled phase for the flow. Conversely, some cases were reported as single-phase, yet the values of thermal-hydraulic parameters suggested a saturated mixture. This verification process covered a total of 736 extracted cases (292 single-phase cases and 444 two-phase cases).

The applied verification process involved:

1. Identifying thermal-hydraulic parameters using the (IAPWS IF-97) steam table, specifically the specific enthalpy values based on pressure and temperature at the inlet and outlet.

2. Determining the thermodynamic quality of the flow before and after the heater by considering enthalpy values, as:

$$x = \frac{h\,(T,P) - h_{saturation,\ liquid}(P)}{h_{saturation,\ vapor}(P) - h_{saturation,\ liquid}(P)} \tag{2}$$

If the quality is negative, it indicates that the flow is sub-cooled (single-phase), and if it is positive, it indicates the presence of voids in the flow (two-phase). Additionally, the temperatures are compared to the saturation temperature at the specific pressure of the case.
The cases are then verified based on the results and the reported phase. Since heat losses are not reported, the following steps aim to estimate the heat losses for each case considering the previous information.

3. Heat losses are calculated using the following two sub-steps:

   If the outlet temperature is lower than saturation, heat balance can be calculated using the measurements of inlet and outlet temperatures at the given pressure:

$$Power_{calculated} = \dot{m}\,(h_{out} - h_{in}) \tag{3}$$

   Then the calculated heat losses:

$$Q_{heat\ Losses}(\%) = \frac{Power_{reported} - Power_{calculated}}{Power_{reported}}.100 \tag{4}$$

   If the calculated outlet temperature is at saturation, the outlet thermodynamic quality can be calculated as:

$$X_{Outlet\ 2\ phase\ Quality} = \frac{h_{in} + \frac{Power_{reported}}{\dot{m}} - h_{saturated,\ liquid}}{h_{saturation,\ vapor}(P) - h_{saturation,\ liquid}(P)} \tag{5}$$

Then the calculated heat losses:

$$Q_{heat\ Losses}(\%) = \frac{X_{reported} - X_{calculated}}{100}.100 \quad (6)$$

The final analysis indicates that several cases exhibited excess heat in the loop. This discrepancy can be attributed to various factors, including but not limited to variations in heater power, uncertainties associated with measurement devises, conducting test cases in rapid succession, and inadequate time intervals between tests, resulting in excess heat stored in the loop's heat structures. Therefore, in this report, the term 'heat losses' refers to either the actual heat lost or positive variations from the reported power values. Considering the above procedure, the list of single-phase cases and two-phase cases has been narrowed down to 268 and 200, respectively. Considering the scope and resources of this activity, the analysis of 52 single-phase cases has been performed earlier in the previous report [3], while this report covers the simulation of 200 two-phase cases.

3. Description of Codes and Simulation Models

3.1 Simulation Codes

Apros is a versatile simulation software conventionally used to design and analyse the dynamic behaviours of power plants and their control systems. Its capabilities encompass comprehensive modelling of various processes within power plants, offering crucial support for verifying and validating power plant designs. Established in 1986 through a partnership between VTT and Fortum's predecessor, Imatran Voima (IVO), Apros features a thermal hydraulics model library encompassing three distinct models for one-dimensional water/steam/gas flow (homogeneous, 5-equation, and 6-equation). Ownership of Apros is shared by Fortum and VTT, with both entities actively engaged in the ongoing development of the code. It also includes models for single-phase flow, containment, and steady-state flow with tank dynamics. With successful references worldwide in approximately 30 countries, Apros is a proven and globally recognized tool in the field [6].

The C-3 code, jointly developed since 1979 by the French Alternative Energies and Atomic Energy Commission (CEA) in collaboration with Électricité de France (EDF), FRAMATOME, and the Institute for Radiological Protection and Nuclear Safety (IRSN), is the foremost French reference for thermal-hydraulic system codes used in nuclear safety analysis. This collaborative effort, enriched by extensive validation, has established C-3 with a robust reputation. Its modular code component library and the generic equation set, grounded in the 6-equation/2-phase flow model, empower it to skilfully simulate various thermal-hydraulic transients [7].

3.1.1 Apros Model

Using the adjusted model depicted in Figure 3 and Figure 4, an Apros model is constructed utilizing built-in components, namely pipes, points, and a tube & shell heat exchanger. The model comprises 57 thermal hydraulic nodes, and the time step is limited to a maximum of 0.001 s to ensure that mass error values remain within the negligible range.

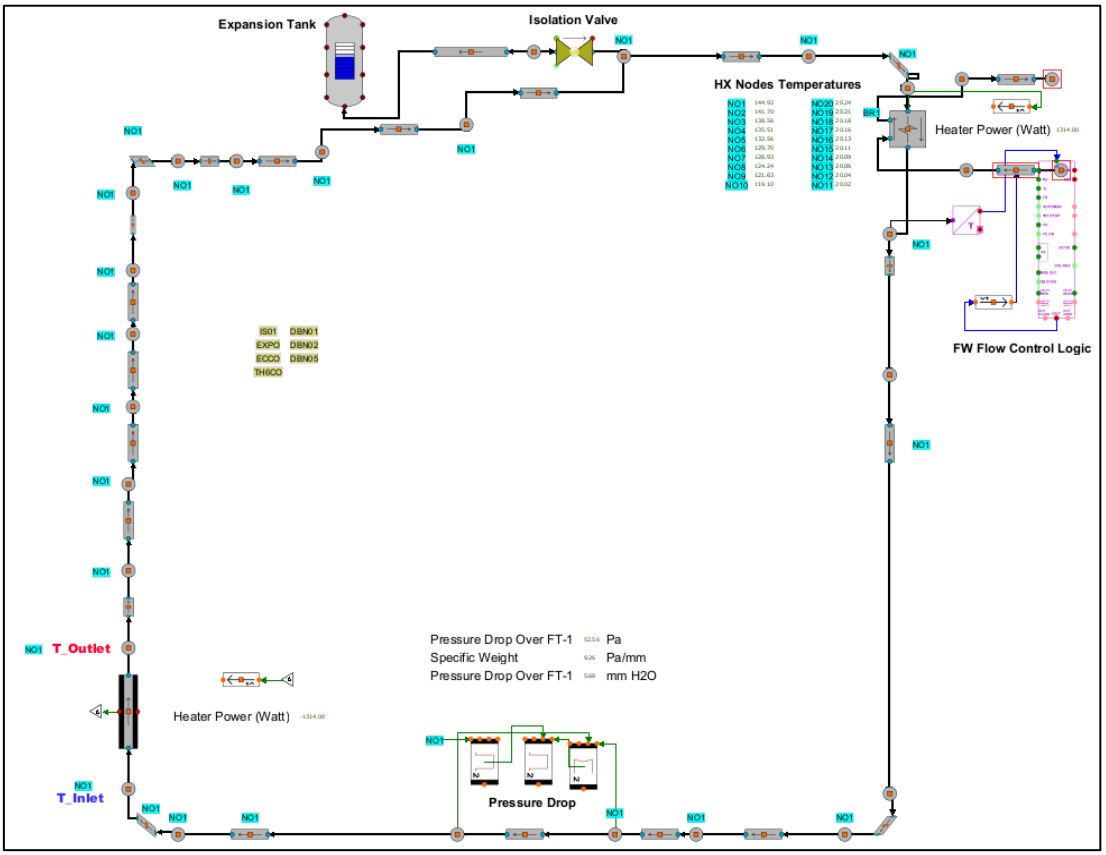

Figure 5: Apros Model Graphical Interface View

The heater is simulated using a Heat Pipe model, emulating the APSARA heater by transferring heat through the heated walls to the fluid flowing inside the pipe. Temperatures (T_{Inlet} & T_{Outlet}) are measured before and after the heater segment. To control pressure during the heating process, an expansion tank is connected to the upper loop leg. Heat is dissipated outside of the system through a heat exchanger, where the secondary side flow rate is automatically adjusted to attain the experimental flow temperature flowing into the heater (T_{Inlet}). To prevent reaching high or low secondary side flow rates necessary for adjusting the temperature out of the heat exchanger, certain cases required tweaking the heat exchanger efficiency to achieve the specified T_{Inlet} values for each test case.
The details provided about the flow measurement device were minimal, so it was assumed, based on the inputs, that the pressure drop is measured over a pipe length of 1 m and converted to millimetres of water column (mm H2O) flow unit at the same temperature. The wall roughness is assumed to be fully smooth, considering a relative roughness of 1.10^{-6} for the loop pipes and heat exchanger. The model is assumed to be fully adiabatic i.e. no heat loss was modelled.

3.1.2 C-3 Model

Using the same adjusted model data, the C-3 model is created in a similar manner, with few differences that are not anticipated to affect the analysis outcomes, such as the pressure adjustment mechanism. Figure 6 illustrates the C-3 nodalization for the adjusted APSARA model.

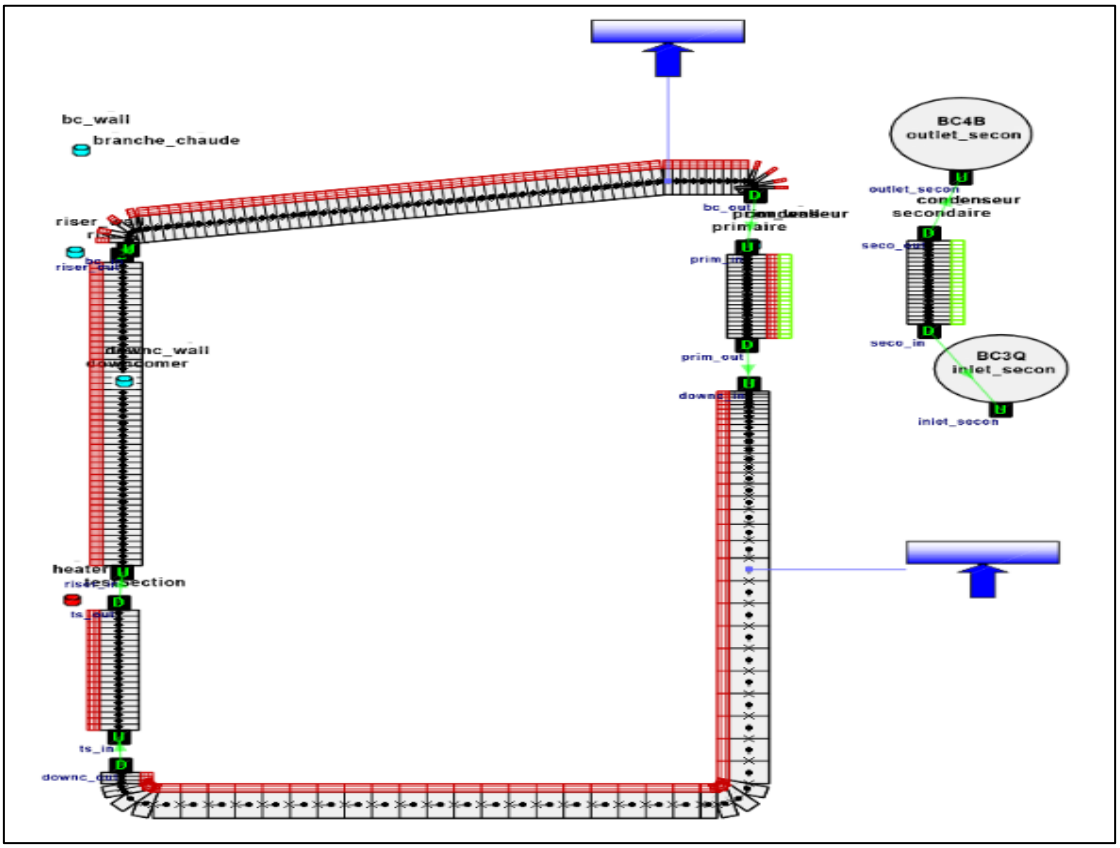

Figure 6: C-3 Model Nodalization

Using the same data and assumptions as in the Apros model, the C-3 model was created. The pipes are modelled using the AXIAL element of C-3, and pipe thicknesses are modelled with the WALL element. However, the corresponding thermal losses are not implemented (they could be added for future studies). The pipe elements are supposed to be adiabatic except for the heat exchanger on the primary side. The heat power is uniformly modelled inside the pipe thickness of the test section (575 mm length). The steam drum geometry and behaviour are not detailed in the report. Therefore, it has been decided to model it as a cross- flow heat exchanger (working as a condenser for two phases cases). The heat exchanger has a length of 400 mm and is consist of two concentric tubes, with the outer channel being the secondary side while the primary side is the internal canal. The tube thickness is 1.8 mm for the internal tube.
The temperature of the secondary side is set at 10 °C. The mass flow rate is adjusted so that the desired test section inlet (T_{inlet}) temperature is achieved. Four singular pressure drop coefficients are implemented, one for each bend. During the APSARA tests, the loop pressure is controlled at the steam drum. In this approach, a pressure control system is implemented, featuring two control valves. The first is located at the top of the loop, and the second is connected to the downcomer element (downstream of the equivalent steam drum). The first valve is set with an opening pressure equals to the experimental test pressure. This control valve enables the draining of the exceeding mass when the temperature increases due to heating. On the other hand, the second valve injects mass if the pressure is below the desired value (the temperature of the injected water is equal to the heat exchanger outlet temperature). The outlet temperature of the heat exchanger is regulated by adjusting the mass flow rate of the secondary circuit using a controller.

4. Results and Discussion

4.1 Background

Natural circulation flow is initiated when the density difference of the fluid between the heat source and heat sink inside the loop creates a buoyancy pressure difference. This difference is balanced by the frictional losses and singular pressure losses. Once the flow rate is established, the driving force is counterbalanced by the pressure losses as follows [8]:

$$\Delta P_{Drive} = \sum \Delta P_{loss} \tag{7}$$

$$\Delta P_{Drive} = -\oint \rho(z) g dz = \sum \Delta P_{loss} \tag{8}$$

$where$:
$\Delta P: pressure\ difference.$
$g: Gravitational\ Acceleration.$

The pressure losses include major losses, namely friction pressure losses, and minor flow losses, which result from bends and geometrical change.

The friction losses along the pipe are estimated using the Darcy-Weisbach equation [9]:

$$\Delta P = f \left(\frac{L}{D}\right)\left(\frac{v^2}{2g}\right) \tag{9}$$

$where$:
$f: friction\ factor.$
$L: Tube\ Length.$
$D: Hydraulic\ Diameter.$
$v: Flow\ Velocity.$

4.2 Apros Analysis

The APSARA facility provided test data across a wide range of cases, conducted at various power levels, heater inlet temperatures, and pressures. The experiments measured key parameters, including flow rate, pressure drop, heater outlet temperature, and void fraction. This analysis focuses exclusively on the two-phase flow cases, comprising 200 scenarios as shown in Table 3. The single-phase cases were analysed separately in a previous report [3]. These 200 two-phase cases were simulated utilizing the 6-equation model, in Apros and results were compared to C-3 simulation outputs received from IRSN. Alpha 1 and 2 refers to measured void in the facility using conductance prob and neutron radiology, respectively. The presented experimental values and the simulation values are averaged values over a steady state due to fluctuation in mass flow rate and the other parameters.

Table 3: Simulated Two-Phase Cases

Run	Tin (C)	Tout (C)	P (bar)	DP (mm H2O)	Power (W)	$\dot{m}$ (kg/s)	X (-)	Alpha1 (-)	Alpha2 (-)
T12-46	183.5	192.9	13.3	13.258	867.00	0.01396	0.0103		
T12-38	186.9	195.2	13.8	22.876	897.00	0.01905	0.0051		
T22-4	156.2	168.2	7.5	15.718	991.0	0.01567	0.00377	0.00000	
T22-3	149.3	168.9	7.4	10.743	1044.0	0.01264	0.00095	0.00000	
T22-5	158.0	168.3	7.5	21.338	1078.0	0.01865	0.00021	0.01226	
T22-6	159.2	169.3	7.5	19.822	1128.0	0.01786	0.00943	0.05426	
T22-7	162.2	171.1	7.6	18.180	1177.0	0.01697	0.01499	0.06226	
T22-8	165.5	173.3	7.7	31.729	1225.0	0.02331	0.00905	0.07053	
T25-27	105.0	118.8	1.3	17.229	1228.0	0.01695	0.0062	0.15330	
T12-36	193.9	198.4	14.5	44.703	1264.00	0.02784	0.0130		
T22-9	168.6	174.3	7.8	41.235	1264.0	0.02704	0.01073	0.18450	
T12-37	193.4	198.0	14.3	44.334	1266.00	0.02772	0.0129		
T25-28	106.0	123.6	1.7	13.892	1286.0	0.01498	0.0053	0.00460	0.02264
T12-43	179.4	192.6	13.2	20.715	1322.10	0.01809	0.0074		
T25-26	97.5	119.1	1.1	12.222	1340.0	0.01397	0.0020	0.14960	
T12-34	194.9	199.5	14.8	47.061	1411.00	0.02865	0.0148		
T12-35	194.3	199.0	14.7	47.137	1423.00	0.02869	0.0148		
T3-5	193.1	207.0	17.7	21.835	1450.00	0.018460	0.008459		
T25-30	109.6	131.4	2.5	10.298	1476.0	0.01259	0.0112	0.00100	0.05063
T12-45	189.5	195.4	13.6	42.426	1497.00	0.02711	0.0146		
T12-44	185.6	194.4	13.4	34.006	1499.00	0.02394	0.0119		
T2-22	206.2	215.1	21.0	30.964	1516.00	0.022000	0.00970	0.03446	
T25-31	113.9	135.5	2.7	12.403	1527.0	0.01398	0.0080	0.00100	
T2-11	209.2	216.3	21.4	44.266	1565.00	0.027000	0.0134	0.01974	
T25-32	117.2	138.7	3.0	13.285	1566.0	0.01452	0.0074	0.00200	
T2-23	208.6	215.8	21.1	36.826	1586.00	0.025000	0.01679	0.11720	
T2-24	210.6	216.7	21.4	41.348	1591.00	0.026000	0.01734	0.17160	
T25-33	121.5	143.6	3.5	14.794	1612.0	0.01541	0.0047	0.03700	
T12-32	194.9	200.4	15.1	48.777	1625.30	0.02925	0.0158		

Run	Tin (C)	Tout (C)	P (bar)	DP (mm H2O)	Power (W)	ṁ (kg/s)	X (-)	Alpha1 (-)	Alpha2 (-)
T15-17	201.4	207.5	17.8	45.425	1629.0	0.0279	0.01618		
T3-9	206.8	214.2	20.0	45.701	1629.00	0.027860	0.017960		
T12-33	195.5	200.4	15.1	48.811	1635.00	0.02925	0.0176		
T15-18	202.5	207.7	17.8	47.833	1637.0	0.0288	0.01750		
T11-10	141.7	160.1	5.3	16.904	1652.00	0.01847	0.01007		
T3-8	205.6	210.7	18.5	46.189	1660.00	0.028100	0.018910		
T11-11	153.4	166.6	6.4	25.007	1664.40	0.02048	0.01169	0.03946	
T3-10	210.3	215.8	20.6	45.778	1667.00	0.027850	0.018580		
T7-4	140.4	152.6	4.2	30.822	1684.00	0.023268	0.00989	0.04820	0.22200
T3-7	199.5	208.6	17.8	36.785	1692.00	0.024780	0.014260		
T3-6	194.9	207.6	17.7	25.741	1704.00	0.020260	0.014010		
T11-12	158.3	168.3	6.7	35.953	1716.90	0.02515	0.01202	0.11600	
T11-13	159.2	169.7	6.9	34.711	1729.00	0.02464	0.01175	0.10440	
T25-35	126.7	152.8	4.5	12.450	1740.0	0.01393	0.0062	0.00040	
T25-34	123.5	153.8	4.9	10.648	1748.0	0.01275	0.0034	0.00060	
T12-14	197.6	203.0	16.1	49.274	1751.20	0.02936	0.0182		
T7-6	153.4	165.4	6.1	31.450	1753.00	0.023364	0.01106	0.07100	0.21260
T12-13	194.5	201.8	15.8	44.949	1766.10	0.02792	0.0156		
T11-15	160.6	171.9	7.3	33.765	1775.00	0.02423	0.01720	0.09560	
T7-5	146.0	156.5	4.7	41.870	1779.00	0.027654	0.09084	0.09153	0.28640
T2-25	206.3	209.7	18.2	47.053	1785.00	0.028000	0.02508	0.29940	
T25-36	127.5	153.6	4.7	12.906	1786.0	0.01421	0.0065	0.00030	
T23-7	144.3	171.3	8.1	12.264	1787.0	0.01368	0.00670	0.00000	
T6-17	209.4	215.6	20.9	44.007	1789.00	0.02743	0.01970	0.21000	
T16-9	158.0	168.8	6.7	38.077	1800.0	0.0260	0.0347	0.11473	
T15-19	203.1	208.2	17.9	48.980	1802.0	0.0291	0.02028		
T6-18	210.3	215.1	20.5	46.832	1802.00	0.02826	0.02250	0.24540	
T16-8	147.9	171.6	7.6	16.685	1802.2	0.0163	0.0333	0.09126	
T11-14	160.3	170.8	7.2	35.618	1804.00	0.02499	0.01274	0.11580	
T15-20	203.2	208.2	17.9	49.461	1804.0	0.0293	0.02049		
T12-31	194.8	200.6	15.2	48.546	1817.00	0.02917	0.0188		
T12-30	192.1	197.5	14.1	48.702	1819.00	0.02929	0.0193		
T12-29	192.2	197.3	14.0	49.313	1821.00	0.02949	0.0199		
T16-10	159.0	166.9	6.9	37.066	1821.0	0.0259	0.0348	0.13920	
T6-20	211.2	216.4	21.1	46.638	1829.00	0.02815	0.02205	0.25420	
T6-21	209.8	214.7	20.4	46.932	1829.00	0.02826	0.02230	0.26180	
T6-22	210.1	215.3	20.6	46.605	1829.00	0.02816	0.02204	0.25900	
T6-19	210.0	215.6	20.8	46.526	1831.00	0.02813	0.02111	0.25000	
T6-23	209.9	215.0	20.5	46.756	1836.00	0.02822	0.02228	0.26230	
T25-37	135.8	160.0	5.7	15.795	1843.0	0.01589	0.0056	0.04180	
T11-16	161.0	172.5	7.5	33.847	1853.00	0.02426	0.01271	0.09820	
T2-26	202.5	206.8	17.1	46.676	1856.00	0.028000	0.02412	0.30580	

Run	Tin (C)	Tout (C)	P (bar)	DP (mm H2O)	Power (W)	ṁ (kg/s)	X (-)	Alpha1 (-)	Alpha2 (-)
T23-8	154.3	172.2	7.3	22.749	1872.0	0.01938	0.00927	0.06200	
T2-27	199.7	204.2	16.1	46.817	1873.00	0.028000	0.02368	0.32340	
T25-38	141.3	168.6	7.2	13.567	1879.0	0.01452	0.0056		
T23-18	162.6	176.1	8.1	29.873	1882.0	0.02255	0.01211	0.06653	
T16-11	159.1	170.3	7.0	37.663	1886.0	0.0258	0.0366	0.10653	
T16-12	160.8	172.3	7.4	36.595	1886.0	0.0254	0.0360	0.13887	
T16-13	161.8	173.0	7.6	36.794	1886.0	0.0254	0.0359	0.14093	
T23-19	162.0	174.5	7.7	33.255	1896.0	0.02399	0.01194	0.08206	
T23-11	160.7	174.3	7.7	30.123	1898.0	0.02268	0.01203	0.07113	0.10040
T23-13	158.9	171.2	7.1	35.084	1898.0	0.02479	0.01124	0.10120	
T23-14	159.3	171.6	7.1	35.230	1903.0	0.02484	0.01114	0.09320	
T23-15	159.9	172.3	7.3	34.430	1914.0	0.02450	0.01180	0.11030	
T23-12	159.6	172.6	7.4	33.228	1916.0	0.02401	0.01142	0.08306	0.10820
T23-9	159.4	172.9	7.4	31.637	1922.0	0.02335	0.01144	0.09000	0.15160
T23-17	163.6	177.4	8.4	28.949	1924.0	0.02213	0.01322	0.06613	
T25-39	143.1	169.1	7.3	14.833	1926.0	0.01526	0.0068	0.00180	
T23-10	158.3	171.0	7.0	34.539	1934.0	0.02457	0.01147	0.09673	0.13720
T23-20	166.0	179.6	8.9	29.887	1942.0	0.02251	0.01309	0.10670	
T23-16	161.0	173.9	7.6	33.192	1946.0	0.02398	0.01235	0.10880	
T7-7	157.7	173.6	7.9	25.060	1952.00	0.020455	0.01322	0.00880	0.11650
T16-14	163.4	175.2	8.1	36.011	1964.0	0.0251	0.0373	0.13507	
T12-16	199.9	205.2	16.8	50.492	1970.40	0.02972	0.0220		
T15-21	203.0	208.2	17.9	49.483	1972.0	0.0293	0.02282		
T6-24	209.9	215.1	20.5	47.337	1977.00	0.02842	0.02436	0.27940	
T12-15	198.6	203.9	16.4	50.453	1983.40	0.02974	0.0223		
T16-15	161.8	175.0	8.0	37.192	2029.0	0.0256	0.0394	0.10120	
T7-8	172.0	184.8	10.5	34.010	2047.20	0.024154	0.00978	0.10550	
T2-10	207.2	215.7	21.2	42.730	2083.00	0.027000	0.0210	0.01824	
T16-16	163.9	176.7	8.4	36.701	2097.0	0.0254	0.0406	0.10727	
T21-7	178.3	200.8	15.5	20.623	2116	0.01805	0.00887		
T23-21	166.6	184.1	10.1	25.287	2153.0	0.02044	0.01441	0.06306	
T6-25	209.9	215.3	20.6	47.535	2156.00	0.02849	0.02704	0.30420	
T7-9	175.1	186.9	11.1	39.743	2161.20	0.026359	0.01490	0.15390	
T21-9	177.3	195.8	13.6	27.217	2163	0.02118	0.01040		
T8-5	229.1	234.2	29.9	47.536	2172.00	0.02800	0.0299	0.26280	
T21-11	180.4	199.0	14.6	25.704	2188	0.02045	0.01247		
T12-28	192.0	197.6	14.1	49.064	2190.00	0.02941	0.0252		
T7-10	177.9	187.0	11.0	45.298	2193.60	0.028361	0.01868	0.26220	
T23-22	165.1	179.7	9.3	32.371	2205.0	0.02358	0.01465	0.05686	
T16-17	165.9	179.9	9.1	34.473	2207.0	0.0244	0.0420	0.11147	
T21-10	177.1	194.4	13.1	27.775	2210	0.02143	0.01348		
T15-22	202.6	207.9	17.7	48.871	2225.0	0.0291	0.02746		

Run	Tin (C)	Tout (C)	P (bar)	DP (mm H2O)	Power (W)	ṁ (kg/s)	X (-)	Alpha1 (-)	Alpha2 (-)
T15-23	200.4	206.3	17.1	48.774	2225.0	0.0291	0.02609		
T21-14	179.4	195.4	13.3	32.312	2228	0.02334	0.01256		
T21-12	179.2	197.2	13.9	27.492	2242	0.02128	0.01302		
T23-23	168.4	184.7	10.5	29.215	2267.0	0.02218	0.01529	0.10340	
T21-13	179.0	196.1	13.6	29.236	2269	0.02204	0.01378		
T21-17	179.0	193.2	12.6	36.408	2274	0.02500	0.01429		
T21-15	178.9	194.2	12.9	33.150	2286	0.02369	0.01459		
T7-11	188.1	196.9	14.1	44.909	2292.00	0.028021	0.02160	0.26510	
T16-18	168.7	185.0	10.5	29.437	2297.5	0.0223	0.0416	0.10167	
T8-6	229.9	235.6	30.8	47.386	2306.00	0.02793	0.0312	0.26000	
T8-7	228.6	233.9	29.7	48.181	2320.00	0.02823	0.0320	0.29350	
T21-18	178.3	192.0	12.1	37.999	2338	0.02563	0.01555		
T6-26	209.9	215.7	20.7	47.533	2361.00	0.02848	0.02992	0.32720	
T12-18	203.0	208.2	17.9	49.801	2362.80	0.02942	0.0296		
T21-19	178.8	192.7	12.3	38.117	2372	0.02567	0.01564		
T6-27	209.2	214.7	20.2	47.406	2372.00	0.02846	0.03098	0.34720	
T12-17	201.6	207.2	17.6	50.085	2387.70	0.02955	0.0290		
T7-12	193.6	203.2	16.5	44.892	2422.00	0.027902	0.02271	0.24450	
T16-19	170.7	191.3	12.3	23.941	2427.0	0.0196	0.0437	0.03133	
T8-8	226.7	234.7	30.1	48.200	2455.00	0.02824	0.0328	0.27400	
T17-3	208.8	214.3	19.9	46.494	2461.0	0.02815	0.03319		
T21-20	178.9	192.9	12.4	38.981	2463	0.02600	0.01660		
T16-20	169.3	188.1	11.3	28.704	2467.0	0.0219	0.0450	0.02607	
T17-2	208.2	213.4	19.7	47.012	2472.0	0.02834	0.03374		
T15-24	201.0	207.3	17.5	48.130	2541.0	0.0289	0.03103		
T15-25	201.3	207.7	17.6	48.064	2554.0	0.0289	0.03109		
T7-13	197.3	207.3	18.1	44.568	2558.24	0.027710	0.02476	0.22500	
T16-21	167.9	184.5	10.3	35.767	2570.0	0.0249	0.0488	0.09187	
T8-9	229.4	235.6	30.7	48.430	2580.00	0.02829	0.0348	0.28320	
T7-14	196.2	206.1	17.6	47.383	2584.00	0.028726	0.02368	0.27520	
T6-28	206.8	215.0	20.4	46.969	2587.00	0.02832	0.03351	0.37010	
T21-21	178.0	192.0	12.1	40.106	2637	0.02645	0.01904		
T17-4	210.2	216.3	20.7	46.407	2648.0	0.02809	0.03560		
T7-15	194.2	204.4	17.0	45.604	2660.00	0.028144	0.02533	0.28780	
T12-21	193.0	199.0	14.6	46.839	2689.00	0.02862	0.0344		
T12-19	197.6	203.5	16.1	47.713	2698.00	0.02883	0.0348		
T17-5	214.4	220.6	22.7	46.630	2714.0	0.02808	0.03661		
T12-20	197.2	203.3	16.0	47.226	2716.00	0.02866	0.0350		
T12-25	192.5	199.1	14.6	47.627	2743.00	0.02890	0.0337		
T7-16	192.7	206.8	16.4	44.126	2759.00	0.027646	0.02689	0.29720	
T15-26	201.5	208.4	17.9	47.413	2803.0	0.0286	0.03491		
T7-17	194.9	206.0	16.9	45.798	2820.00	0.030525	0.02217	0.29290	

Run	Tin (C)	Tout (C)	P (bar)	DP (mm H2O)	Power (W)	ṁ (kg/s)	X (-)	Alpha1 (-)	Alpha2 (-)
T15-27	201.5	208.6	18.0	47.310	2835.0	0.0286	0.03518		
T17-6	217.1	223.6	24.1	46.693	2877.0	0.02822	0.03910		
T8-10	228.6	235.2	30.4	49.008	2879.00	0.02851	0.0391	0.32360	
T7-18	195.4	206.4	17.0	46.013	2937.00	0.028262	0.02837	0.29620	
T17-7	221.1	227.9	26.3	46.922	2949.0	0.02801	0.04043		
T12-24	192.5	199.4	14.7	45.718	2952.00	0.02823	0.0378		
T6-29	208.3	215.1	20.4	45.938	2964.00	0.02797	0.03992	0.50650	
T12-22	192.3	199.2	14.7	45.860	2996.00	0.02829	0.0385		
T7-19	192.3	203.6	16.0	45.428	3013.00	0.028120	0.02927	0.32490	
T17-8	223.6	230.5	27.6	46.884	3063.0	0.02794	0.04283		
T17-9	223.6	230.5	27.6	46.704	3066.0	0.02787	0.04307		
T8-11	227.9	234.8	30.1	42.829	3080.00	0.02640	0.0471	0.31980	
T6-30	207.9	215.0	20.3	45.743	3110.00	0.02791	0.04197	0.44900	
T8-12	230.8	238.2	32.1	48.632	3219.00	0.02833	0.0443	0.35340	
T15-28	200.9	208.6	17.9	45.667	3248.0	0.0280	0.04266		
T15-29	200.5	208.2	17.8	45.595	3287.0	0.0280	0.04329		
T17-10	223.8	230.7	27.7	46.088	3304.0	0.02766	0.04838		
T1-16	228.0	240.4	33.4	47.610	3397.00	0.028100	0.0353	0.24850	
T8-13	231.9	239.1	32.6	48.468	3416.00	0.02824	0.0488	0.36420	
T17-11	223.0	229.4	27.2	45.717	3472.0	0.02755	0.05303		
T1-17	228.7	241.4	34.0	47.745	3478.00	0.028100	0.0363	0.24740	
T1-15	222.8	236.8	31.3	47.647	3491.00	0.028200	0.0327	0.25430	
T8-14	231.3	238.8	32.4	47.763	3628.00	0.02802	0.0531	0.42890	
T15-30	198.8	207.5	17.5	44.242	3634.0	0.0278	0.04861		
T15-31	198.9	207.7	17.6	43.731	3655.0	0.0274	0.04906		
T17-12	223.1	229.2	27.4	45.061	3707.0	0.02732	0.05907		
T17-13	222.5	228.8	27.2	43.854	3747.0	0.02691	0.06026		
T8-15	231.4	239.4	32.7	47.558	3832.00	0.02795	0.0564	0.42790	
T14-22	214.6	232.6	29.3	46.412	3894	0.028	0.03089		
T14-20	211.4	229.6	27.7	46.183	3934	0.02799	0.03107		
T8-16	232.3	240.2	33.2	46.955	4039.00	0.02772	0.0612	0.45110	
T15-32	198.7	207.7	17.8	42.342	4052.0	0.0269	0.05761		
T4-17	217.2	235.2	30.7	49.516	4055.00	0.028979	0.03401		
T14-24	212.7	231.5	28.6	47.770	4186	0.02851	0.03317		
T8-17	231.8	240.3	33.2	46.525	4311.00	0.02759	0.0659	0.48480	
T17-14	222.6	228.6	27.1	43.198	4376.0	0.02668	0.07473		
T8-18	231.2	240.8	33.6	45.624	4483.00	0.02730	0.0676	0.49200	
T8-19	230.2	238.5	32.1	44.632	4655.00	0.02698	0.0753	0.48730	
T17-15	221.4	228.0	26.8	40.998	4694.0	0.02592	0.08263		
T8-20	234.3	242.2	34.6	44.284	4801.00	0.02676	0.0810	0.49660	
T10-18	238.5	247.5	38.0	46.160	4979.00	0.02730	0.081	0.47430	
T17-16	221.8	229.2	27.3	41.165	5058.0	0.02596	0.06839		

Run	Tin (C)	Tout (C)	P (bar)	DP (mm H2O)	Power (W)	ṁ (kg/s)	X (-)	Alpha1 (-)	Alpha2 (-)
T10-19	238.1	247.2	37.9	45.067	5263.00	0.02700	0.103	0.48330	
T17-17	222.4	230.2	27.7	40.489	5319.0	0.02571	0.09433		
T10-20	238.4	246.8	37.6	45.188	5416.00	0.02700	0.093	0.48570	

The analysis investigates multiple boundary conditions and geometrical modifications to develop a preliminary understanding of the two-phase natural circulation phenomena and the code's simulation response to these changes. The first simulation run was conducted using a 250 mm HX, with regulating inputs to the HX secondary-side flow taken from the point immediately before the heater (highlighted by a red circle)[3]. The second analysis set utilized a 400 mm HX, with regulating inputs sourced from the same location as in the first run.

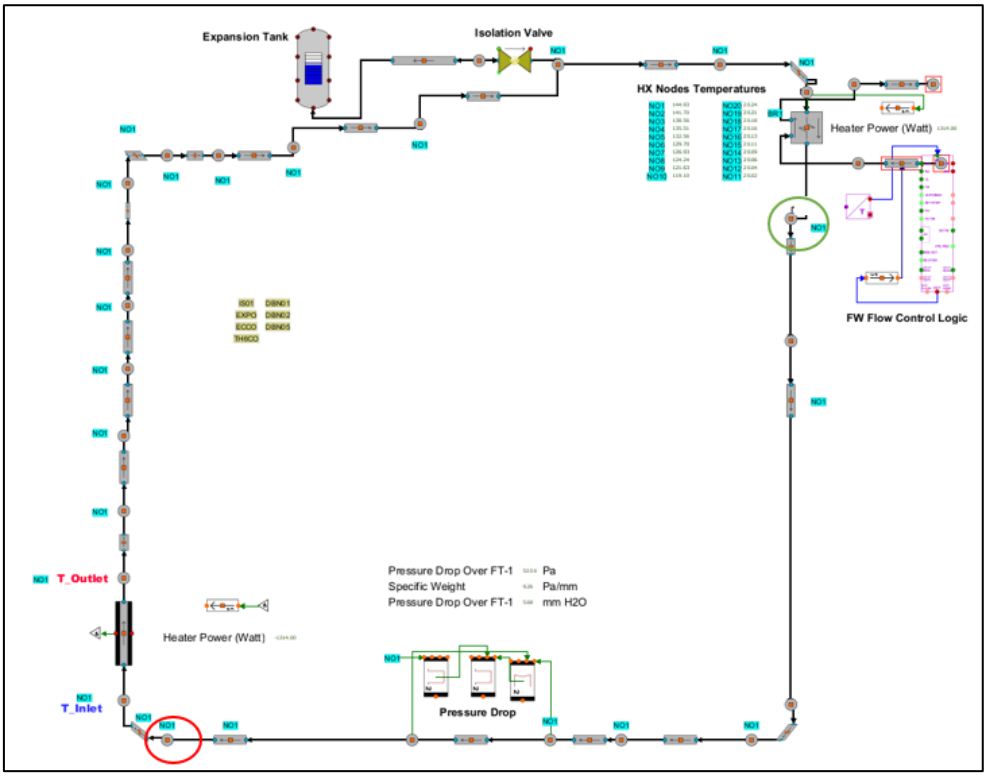

Figure 7: HX Flow Control Logic Input

4.2.1 First Analysis Round (250 mm HX)

This first set of investigation started using the same model and logics adopted in simulating the single-phase cases [3], except that the regulating inputs for the secondary side of the HX (FW flow Control Logic) are taken from the heater inlet. The reason for this change is originated from an initial investigation showed that once the regulation inputs are taken from the HX outlet, the cases behaviour tend to be more unstable

[3] Before the "First analysis Round", full analysis to the 200 cases was performed using the input to the HX flow control logic form the point after the HX (highlighted in green) as performed with single-phase analysis in [3]. However, this input increases the fluctuation as it would be further detailed in sub-section "Effect of Hydrostatic Pressure Inside the Loop". This initial round is not presented in the report.

because of the logic response that is regulating the HX secondary side flow. To avoid this issue, the controller inputs have been changed to the heater inlet where temperature and fluctuation is more stable, enabling the code user to focus on the behaviour physics avoiding the noise generated by the regulation logic. In this analysis the convergence criteria were set by the user to be that the temperature inlet variation does not exceed -/+ 0.5 C. The analysis yielded 144 cases[4] that met the identified convergence criteria. Figure 8 and Figure 9 show the calculated outlet temperature by Apros (250 mm HX) in comparison to the experimental facility's data. The figures show that the outlet temperature is underestimated by a maximum deviation of -5.3 %. The deviation percentage tends to decrease with power increase.

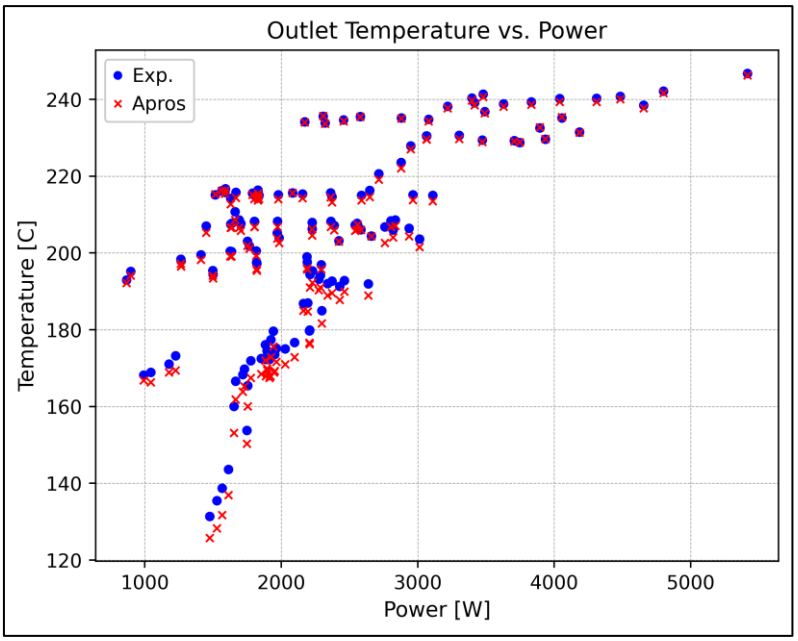

Figure 8: Outlet Temperature (250-mm HX)

[4] The convergence cases number is conservative, as there were many cases omitted during the data processing due to small deviation in other input parameters such as pressure or power.

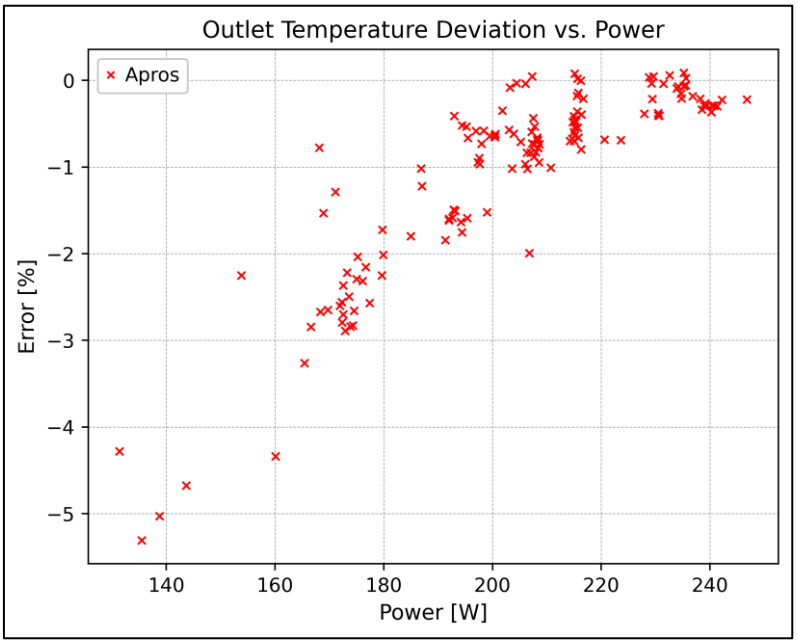

Figure 9: Outlet Temperature Deviation (250-mm HX)

The pressure of the system is a user-controlled parameter, and as evident in Figure 10, achieving steady state at the desired pressure value was generally accomplished to facilitate a proper data simulation.

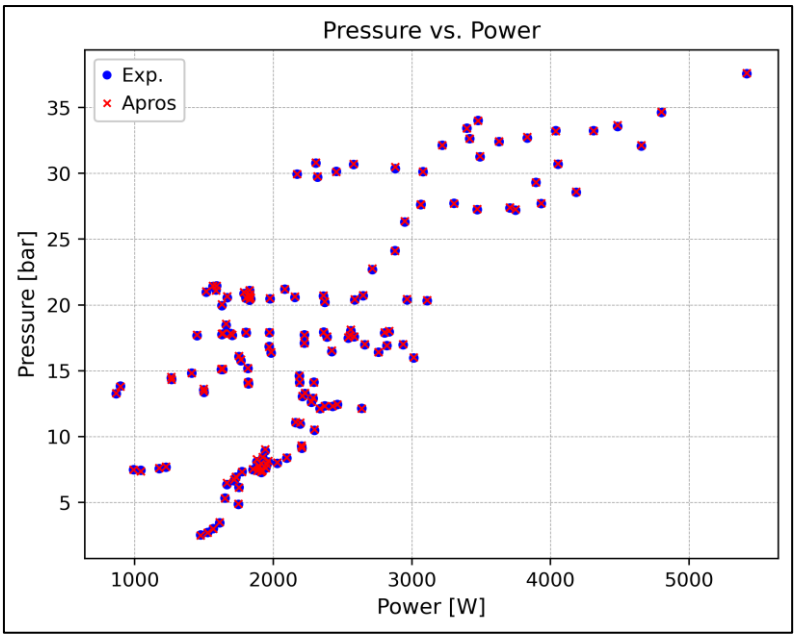

Figure 10: System Pressure (250-mm HX)

Figure 11 and Figure 12 reveal that the code has generally overestimated the flow rate in most cases, with mean deviation value of 25.5 %, which can explain the underestimation of the outlet temperature shown in Figure 8.

This discrepancy can be linked to assumptions made during the modelling process, particularly the omission of the condenser setup, which significantly impacts the state of the coolant flowing to the heater. In the APSARA facility, specifically with the steam drum configuration, the flow leaving the bottom of the

steam drum consists purely of liquid. However, in the simulation, some cases show the exiting coolant still in a two-phase state. Furthermore, elevation and geometrical assumptions have a direct impact on the driving force. Other factors, such as heat losses, water level inside the omitted steam drum and friction losses, also influence the driving force.

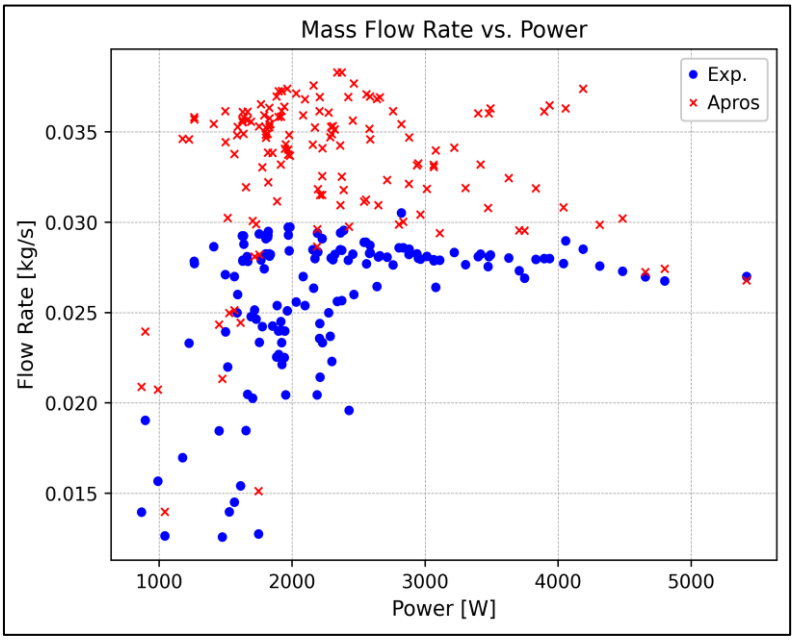

Figure 11: Mass Flow Rate (250-mm HX)

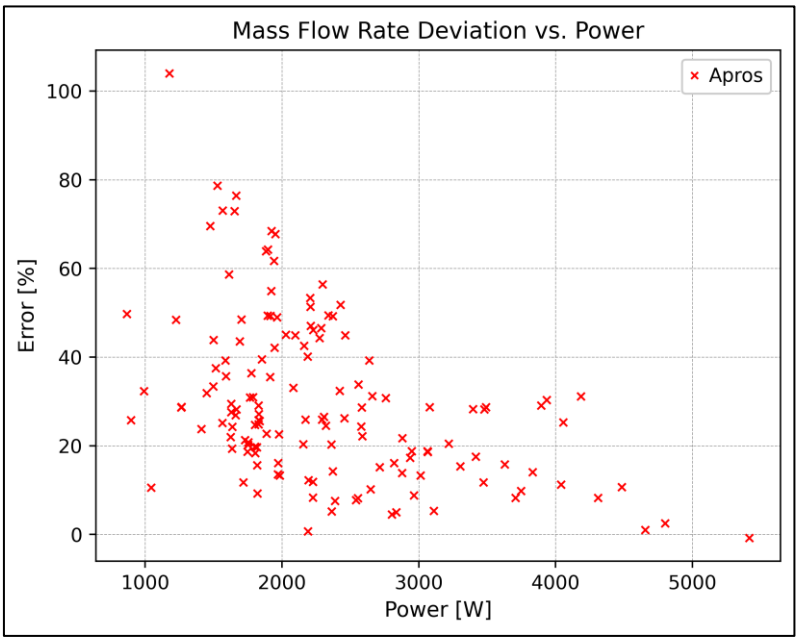

Figure 12: Mass Flow Rate Deviation (250-mm HX)

Figure 13 shows the void fraction generated by the heater, which was overestimated, despite the under estimation of the outlet temperature, indicating that other factors might influence this overestimation such as pressure drop over the heater and heat losses.

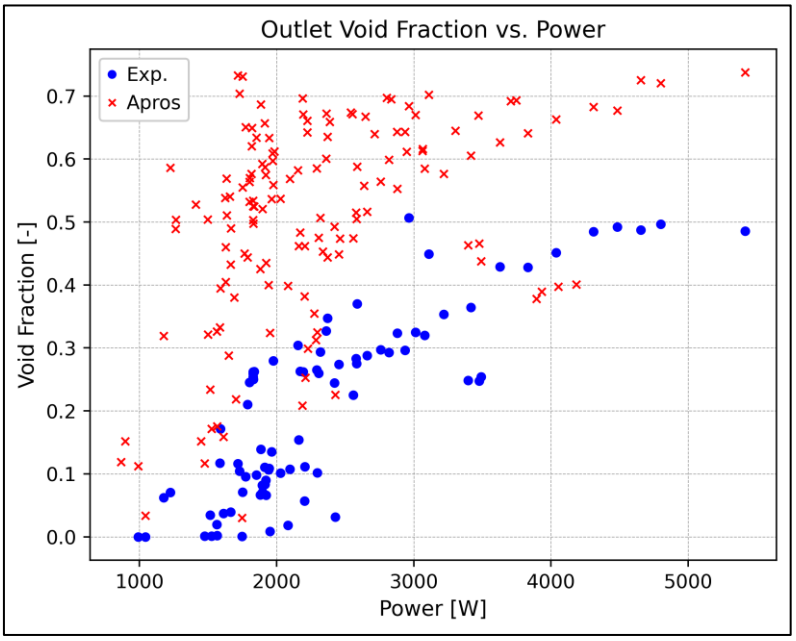

Figure 13: Void Fraction (250-mm HX)

Effect of Hydrostatic Pressure Inside the Loop

It has been observed that condensation and void generation within the loop are influenced by hydrostatic pressure, which in turn affects the overall behaviour of the coolant flow, particularly in the riser and downcomer. This is an important consideration when designing natural circulation-based safety systems, as the height of the riser and downcomer can be adjusted to account for these phenomena. In general, increasing the downcomer length increases the hydrostatic pressure difference, supporting steam condensation if any steam remains after passing through the HX. On the other hand, increasing the riser height leads to higher void generation, which is directly linked to an acceleration of the coolant flow.

Figure 14 shows the void fraction both before and after the HX. The figure demonstrates that the length of the HX is insufficient to condense all the void generated by the heater. However, as the void moves downward through the downcomer, the increasing hydrostatic pressure leads to condensation, transforming the coolant into a fully subcooled state, as shown in Figure 15. In addition, the interfacial friction between the steam and liquid droplets is governed by models and correlations which require further studies to see the effect that these options can contribute to the overall behaviour.

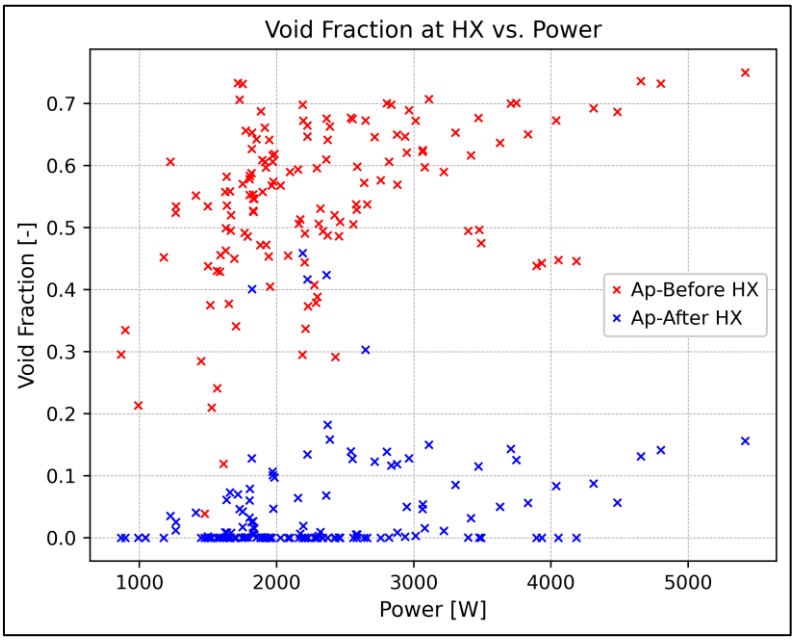

Figure 14: Void Fraction at HX Location (250-mm HX)

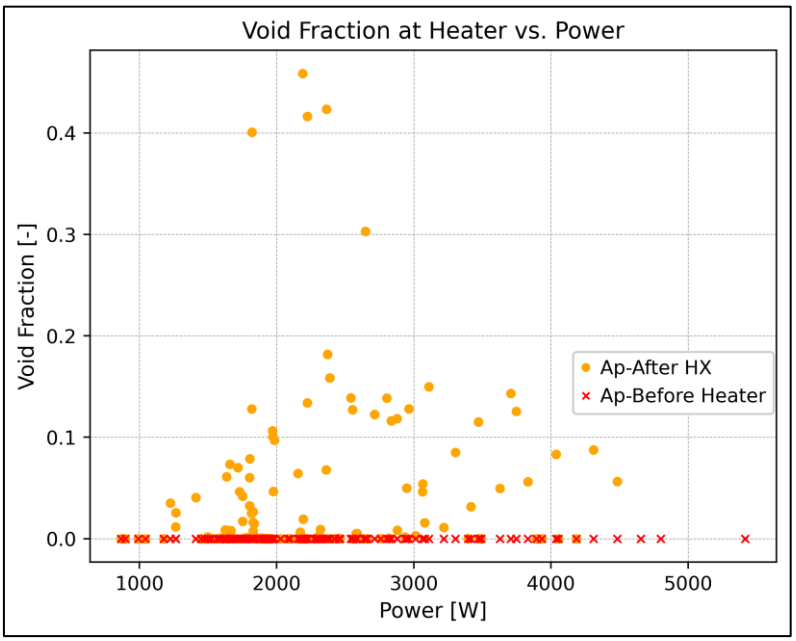

Figure 15: Void Fraction at Heater Location (250-mm HX)

Figure 16 shows a comparison between two cases showed noticeable variation in temperature profile (plotted in RED) and one case that showed no significant variation (plotted in GREEN). points 5 and 6 represent the start and end of heater, points 19 and 20 represent the HX, while 12 to 19 represent the upper horizontal pipe. In the case shown in green, the temperature outlet from the HX is kept constant through the downcomer until it reaches the heater inlet, while the other cases show variation in temperature between the HX outlet through the downcomer until it reaches the heater. This temperature variation is stemmed from the fact that steam and liquid exchange heat along the way in addition to the condensation occurs due to hydraustatic pressure. The point emphasized by this figure is that temperature variation in the planned test facility should not always be linked to heat losses, and thus measurement devices should always be comprehensive to provide full picture of the behaviour for the analysis.

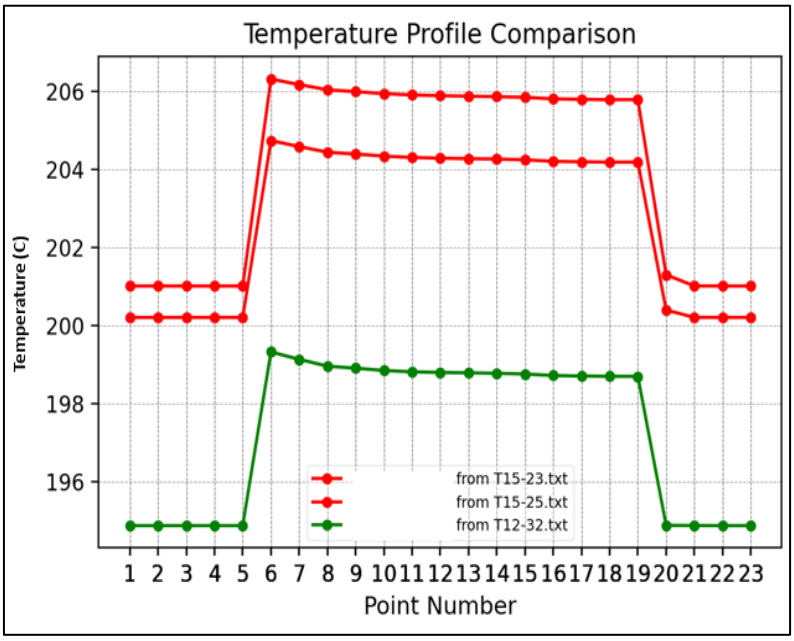

Figure 16: Temperature Profile Comparison of Three Cases (250-mm HX)

The following figure supports the previous one by showing the presence of voids inside the loop. The red cases indicate the presence of void after the HX, which reinforces the conclusion of heat exchange between steam and liquid in the downcomer and its impact on the temperature variations observed in the simulation results. The figure highlights the void fraction in the riser section (points 6–11), where the void fraction increases due to the reduction in pressure as steam rises through the riser, until it enters the inclined horizontal pipe. In the inclined horizontal pipe, two factors are competing. First, the steam occupies the upper part of the pipe, while the liquid occupies the lower part. This arrangement increases the interfacial heat transfer area between the two phases, promoting condensation. However, the pipe is inclined at a positive angle, meaning that as the coolant moves toward the HX, it gains elevation, resulting in a reduction of hydrostatic pressure and more evaporation will occur. It is believed that these two factors are competing to produce the void presence shown in the Figure 17.

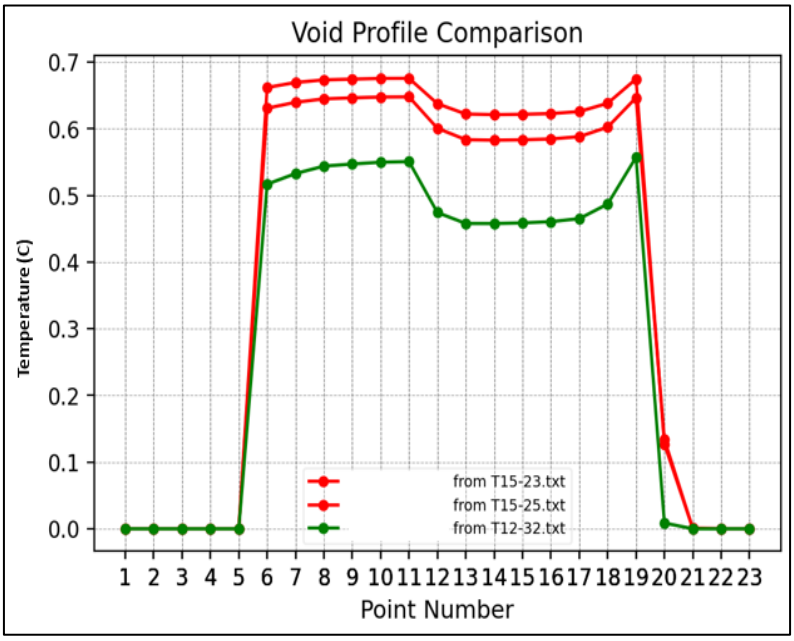

Figure 17: Void Profile Comparison of Three Cases (250-mm HX)

4.2.2 Second Analysis Round (400 mm HX)

The work continues to investigate the effect of the HX length toward the overall phenomena, specially when it comes to HX exit void presence. Thus, it has been decided to repeat the study using 400 mm HX length, by adding 150 mm to the HX and reducing it from the downcomer length, in order to conserve the model overall elevation. Due to time limitation, the full set of cases could not be run, and only 124 cases have been simulated. The convergence criteria have been used as in the first round and it has been observed that simulation convergence is generally faster.

The outlet temperature is underestimated a shown in Figure 18, with tendency of reduced deviation at high temperatures.

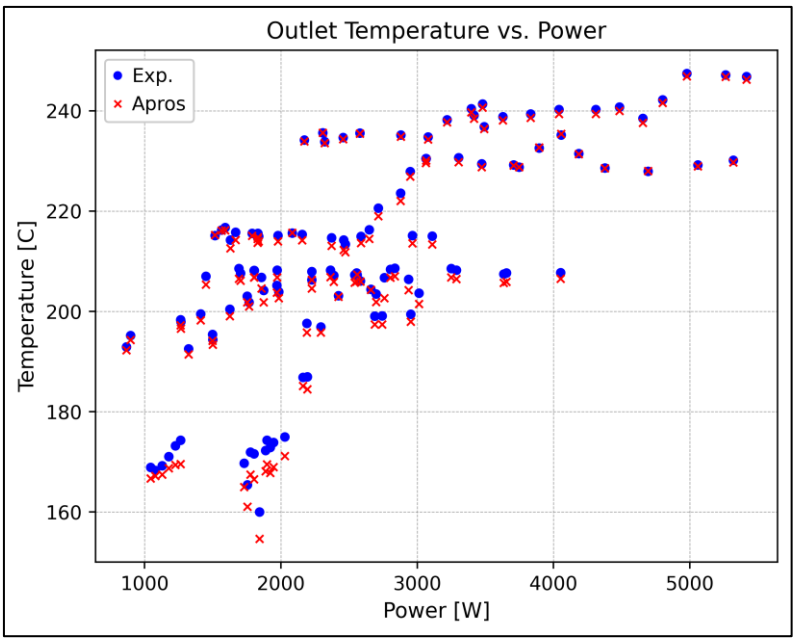

Figure 18: Outlet Temperature (400-mm HX)

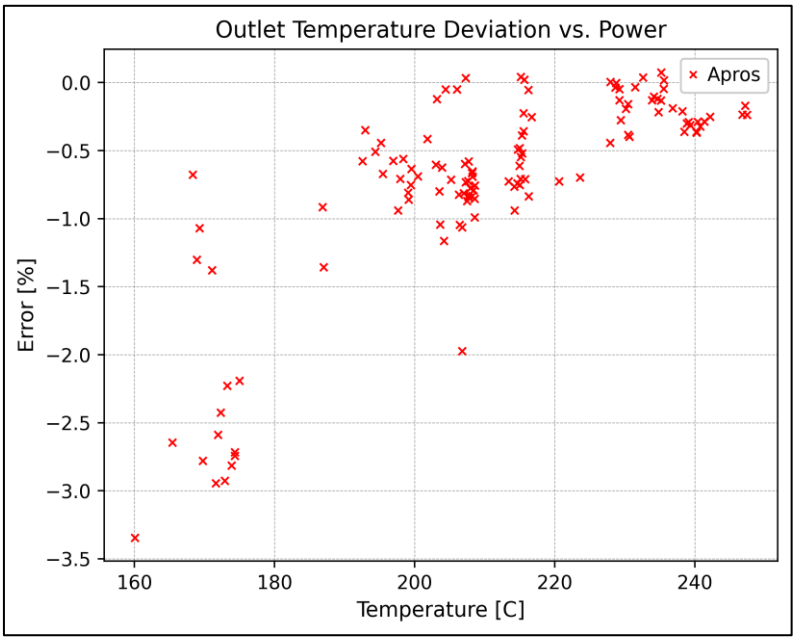

Figure 19: Outlet Temperature Deviation (400-mm HX)

The pressure is controlled as previously performed and can be seen in the following figure.

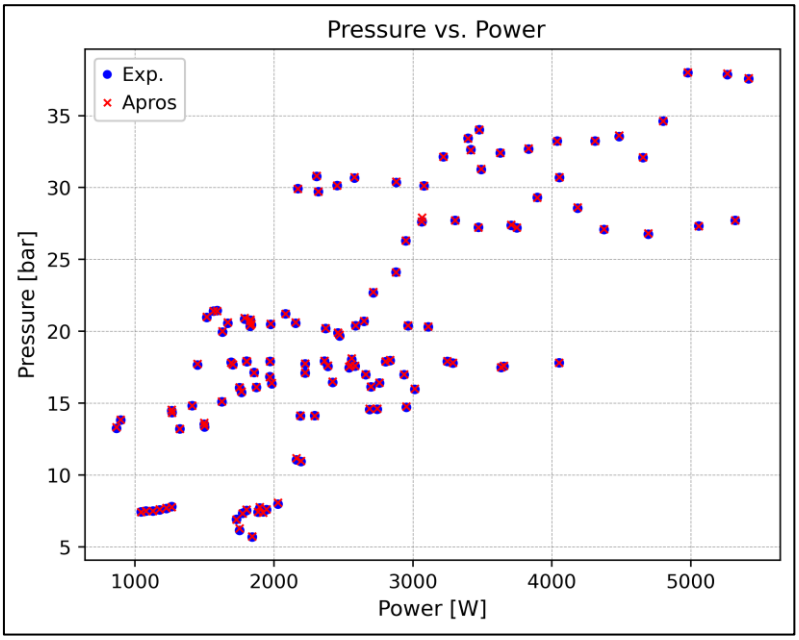

Figure 20: System Pressure (400-mm HX)

Figure 21 shows the mass flow rate is generally overestimated, however, unlike in the first round, there are some cases where underestimation can be observed. These cases could not meet the convergence criteria in the first round, and for that the comparison is not possible with the first round. These cases are characterized generally by the presence of high void after the HX and despite they condense fully before entering the heater (Figure 24), it is believed that this is the reason of the deviation beside the location of the FW logic input. Figure 22 shows the mass flow rate deviation from the experimental data.

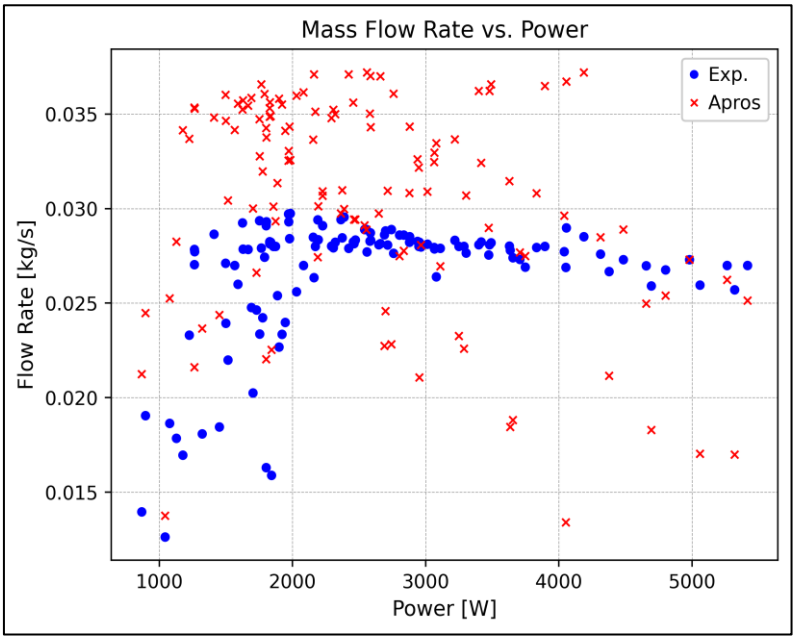

Figure 21: Mass Flow Rate (400-mm HX)

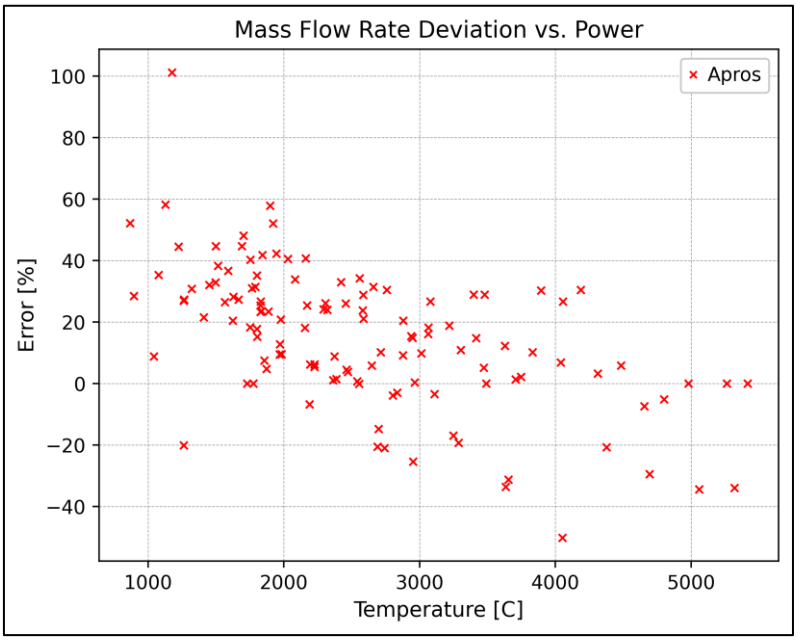

Figure 22: Mass Flow Rate (400-mm HX)

Figure 23 shows the void generated by the heater compared to the experimental data[5].

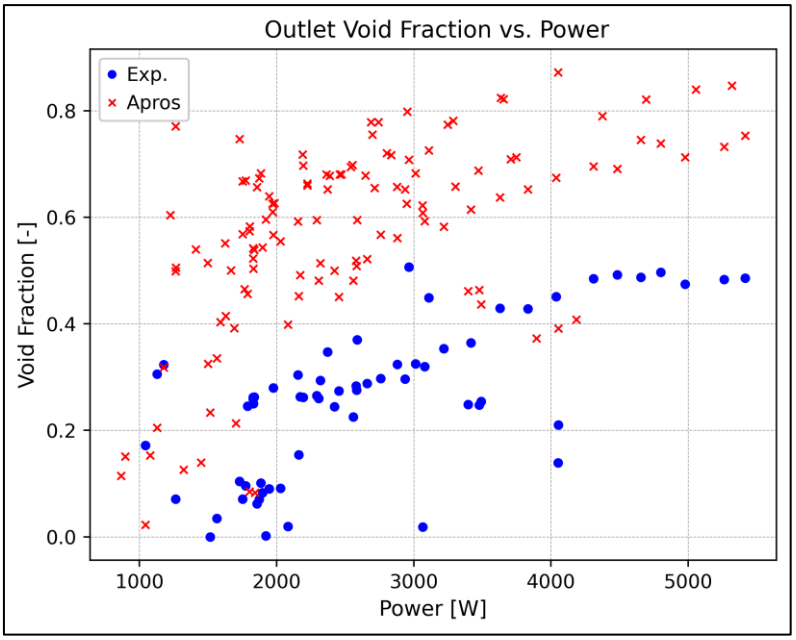

Figure 23: Void Fraction (400-mm HX)

[5] Not all the experimental data included in this simulation have reported values for the void presence.

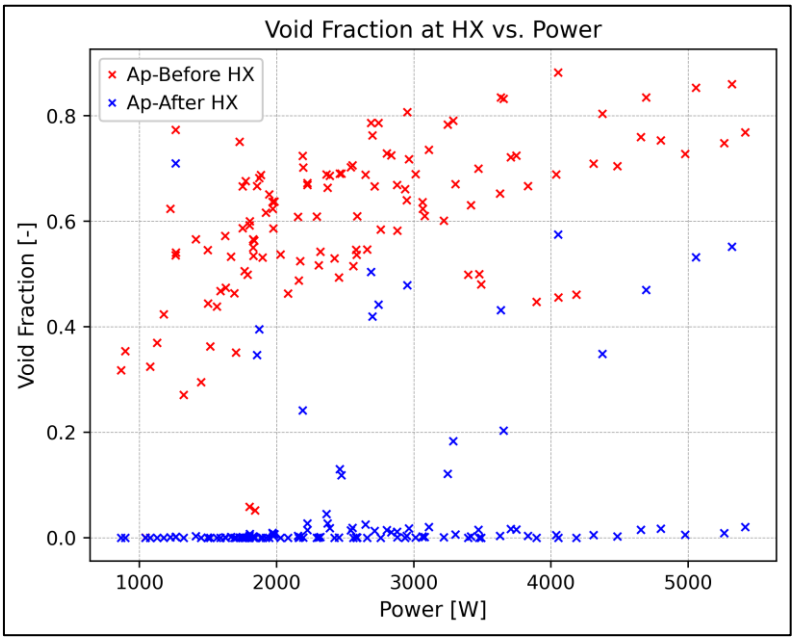

Figure 24: Void Fraction at HX Location (400-mm HX)

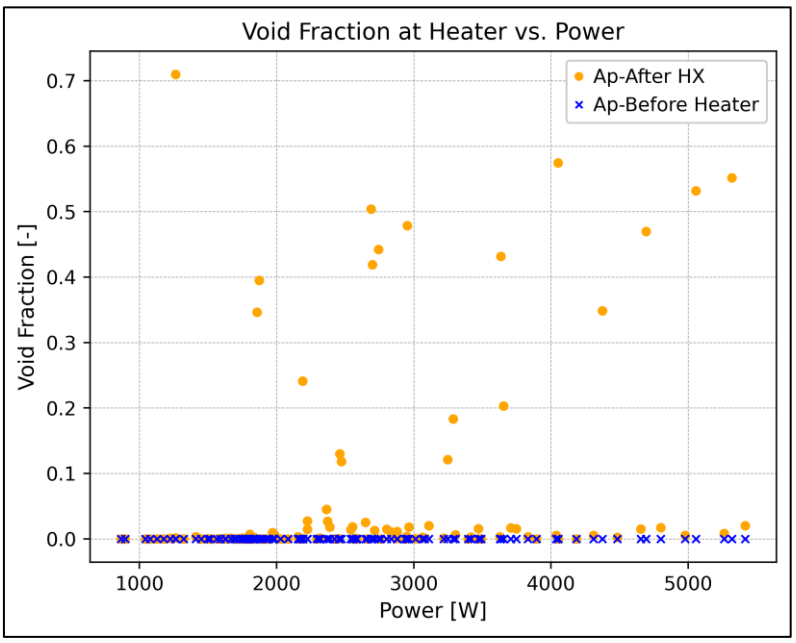

Figure 25: Void Fraction at Heater Location (400-mm HX)

Comparison to 250 mm HX

This sub-section shows the deviation percentage comparison between the simulation of Apros model HX 250 mm and 400 mm regarding the outlet temperature and the flow rate. Since both rounds yield different number of simulated cases, only matching cases are shown in the following figures. The deviation percentage tend to be close to each other with no major deviation from each other, while Figure 27 shows comparison between the mass flow rate deviation in both simulation and it can be observed that generally the 400 mm HX yielded less deviation than the 200 mm HX.

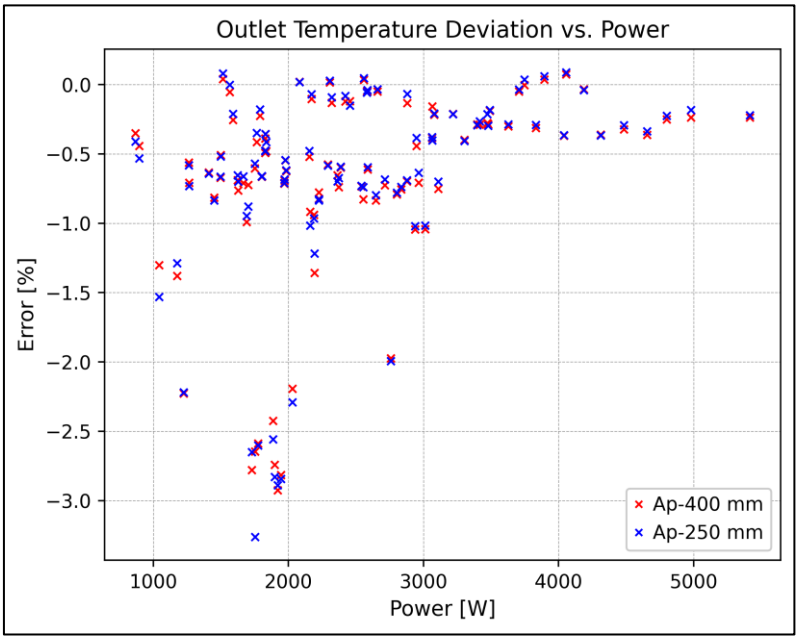

Figure 26: Outlet Temperature Deviation (Apros)

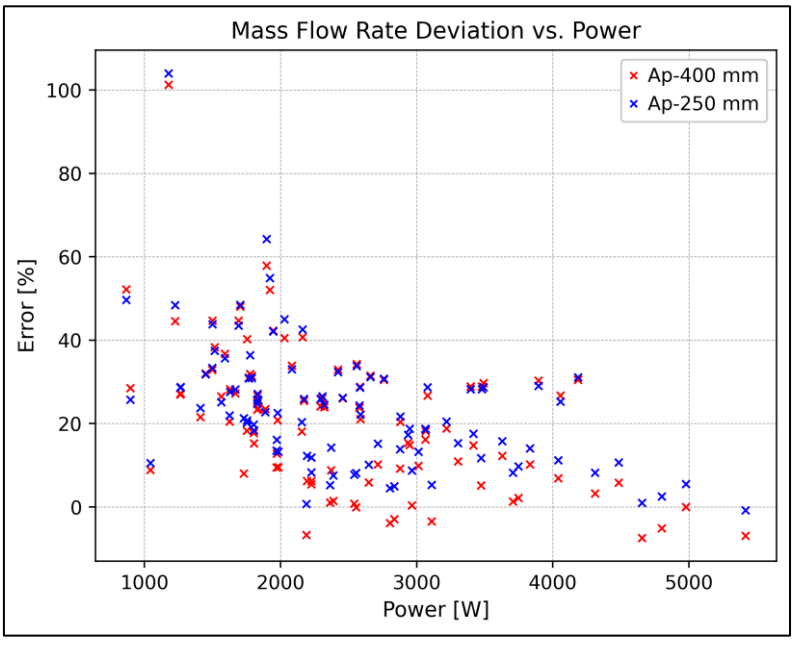

Figure 27: Mass Flow Rate Deviation (Apros)

Frequency analysis

Two-phase flow is characterized by fluctuations arising from the presence of voids in the flow, which influence other thermal-hydraulic parameters. The cases simulated in this study show such fluctuations, and this section aims to identify the dominant frequencies of these fluctuations using Fast Fourier Transform (FFT) [10]. The analysis is performed for the simulated cases using the 400 mm HX. The analysis presented below was performed on a steady-state simulation over a 100-second period, with data recorded at a time step of 0.2 seconds. The frequency is calculated to measure the fluctuation in the mass flow rate.

Figure 28 shows the dominant frequency as a function of power. An initial observation indicates that mass flow rate fluctuations are more observed at lower power levels (<2200 W). However, it is more insightful to associate these fluctuations with the void fraction (Figure 29), as the experiments were conducted under varying pressure conditions. The results suggest that mass flow rate fluctuations generally increase with void fraction up to approximately 50 %, after which they tend to decrease as void fraction exceed this threshold.

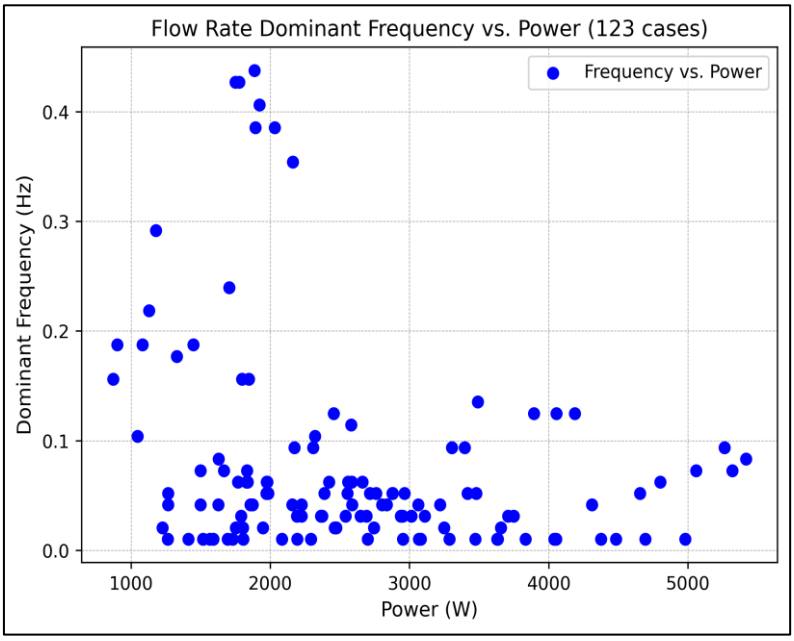

Figure 28: Dominant Frequency Vs. Power (400 mm HX)

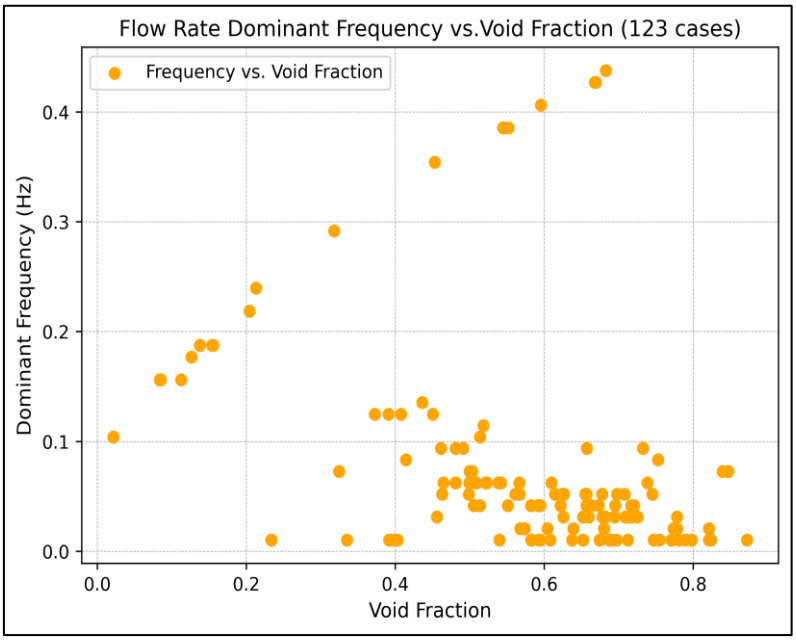

Figure 29: Dominant Frequency Vs. Void Fraction (400 mm HX)

Figure 30 shows the relationship between the fluctuation frequency and amplitude with respect to power. At lower power levels, higher frequencies and larger fluctuation amplitudes are observed. on the other hand, at higher power levels, both the amplitude and frequency of fluctuations tend to decrease.

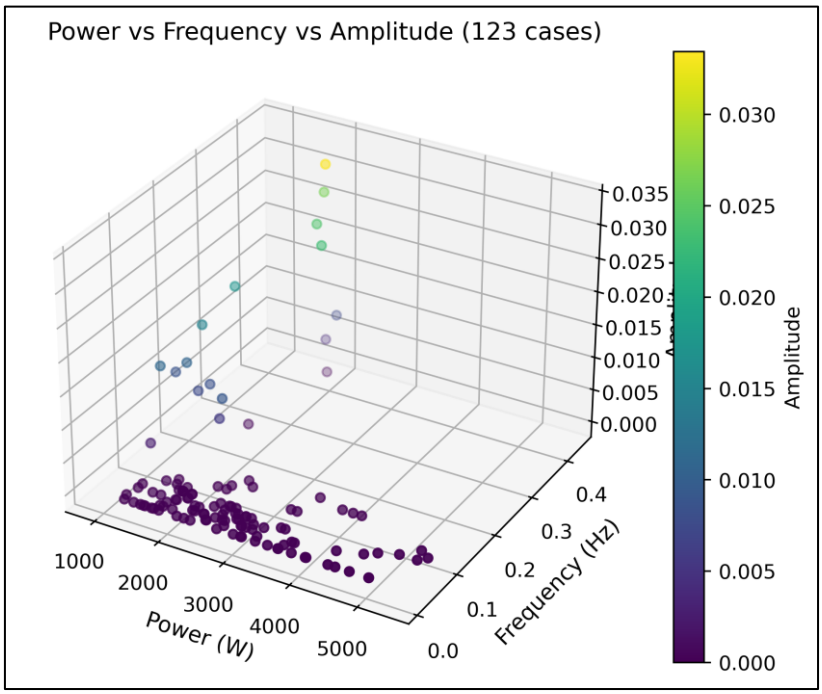

Figure 30: Dominant Frequency and Fluctuation Amplitude Vs. Power (400 mm HX)

This frequency analysis highlights areas for further investigation to enhance our understanding of the system dynamics. Future work could include examining density wave oscillations, flow regime transitions, and numerical stability to build upon these findings.

Code-to-Code Comparison

These two-phase cases were simulated using Apros and C-3. A total of 87 cases can be compared on the 400 mm HX arrangement, as Apros and C-3 yielded different numbers of converged cases due to convergence criteria and time limitations. Figure 31 shows that both codes predicted the outlet temperature with a satisfactory level of accuracy, and the underestimation tends to decrease as the power increases.

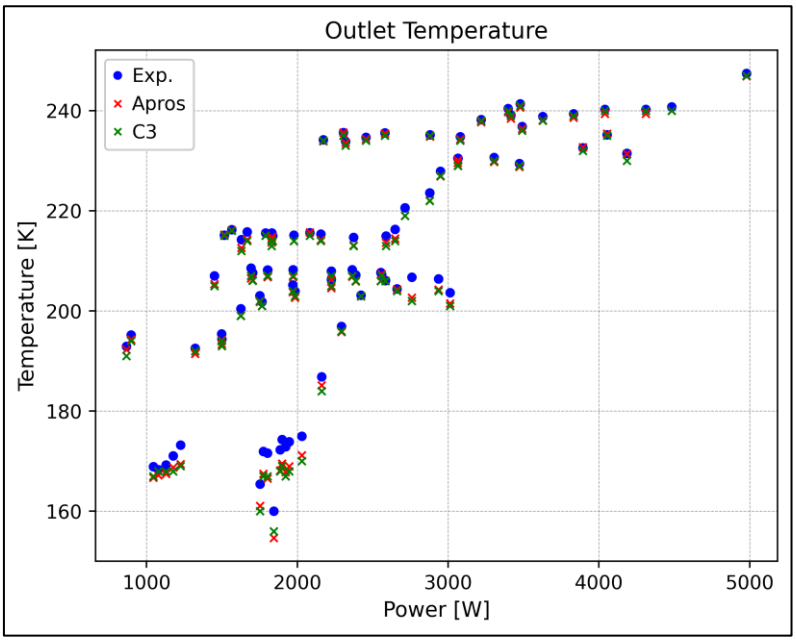

Figure 31: Outlet Temperature (Apros and C-3)

Figure 32 shows that both codes overestimated the mass flow rate; however, the overall behaviour mirrors the experimental trend.

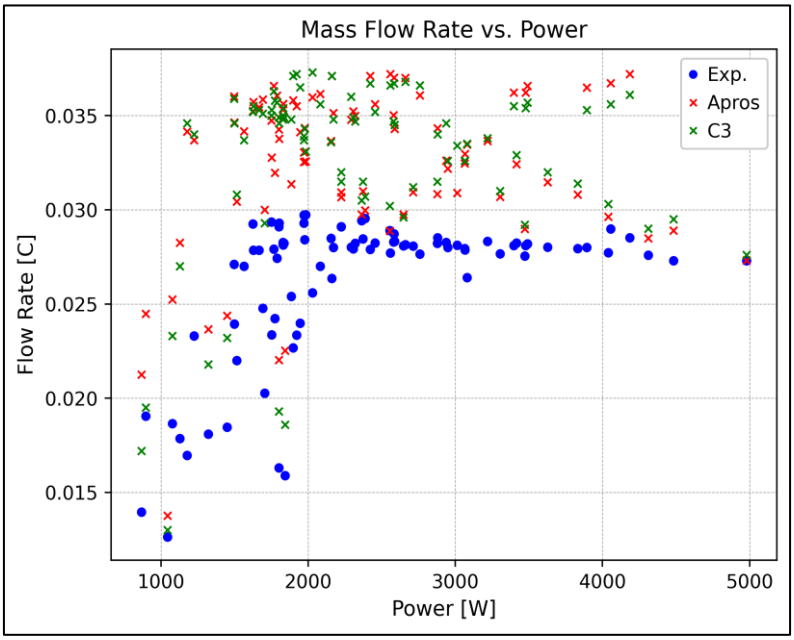

Figure 32: Mass Flow Rate (Apros and C-3)

4.3 Discussion

Simulations of 200 two-phase cases were conducted using Apros with two different HX geometries: a 250 mm HX and a 400 mm HX. Generally, both configurations revealed consistent overestimation of mass flow rate and void generation, alongside underestimation of outlet temperature. However, in the 400 mm HX setup, certain cases deviated by underestimating the flow rate.

While the original APSARA facility ensures pure liquid flow from the steam drum outlet, this exercise neglected this constraint to focus on evaluating HX length and the associated phenomena under these configurations.

To analyse and compare the results, a user-defined convergence criterion was applied. This criterion required heater inlet temperature variations to remain within ±0.5°C. Due to fluctuations in mass flow rate and other parameters, the number of “converged” cases differed between the two HX setups, and only matching cases were compared. Note that the convergence in this context refers not to numerical stability but to satisfying the user-defined criteria for reduced fluctuations. Differentiating physical fluctuations from numerical ones was challenging and remains a limitation of this study.

Key Simulation Challenges

One critical factor influencing thermal-hydraulic behaviour and convergence was the location of input data feeding the feedwater control logic that control the secondary side flow of the HX. In the model, the feedwater flow for the HX secondary side is automatically adjusted based on temperature input from a specific point in the loop to meet target inlet temperatures. Two challenges were identified:

1. **Control Logic Fluctuations:** when the feedwater control logic used temperature input from immediately after the HX (as were performed in the single-phase simulation), some cases exhibited high mass flow rate fluctuations and consequently fluctuation to other parameters. These fluctuations stemmed from the controller's rapid response to temperature changes at this location.

2. **Pressure Drop Effects:** in the simulation, the feedwater of the HX is adjusted to achieve a certain heater inlet temperature at the downcomer (two options were investigated, one after the HX immediately, and the other option adopted by the two rounds, shown in section 4.2.1 and 4.2.2 are at the point before the heater). imposing strict temperature control immediately after the HX caused significant pressure drops, especially in the shorter 250 mm HX. This disturbed the flow behaviour and hindered convergence.

These findings emphasize the importance of selecting stable input locations and comprehensively testing control logic configurations. In addition, comprehensive measurement devices in testing facilities are important for verifying the occurrence of these phenomena at different points within the loop.

Insights on Flow Phenomena

Neither of the HX configurations ensured complete condensation of two-phase flow under the present uncertainties and assumptions. As a result, varying amounts of steam were observed at the HX exit, contrary to the APSARA setup where the steam drum outlet is fully liquid. Despite this limitation, the analysis revealed valuable insights:

- **Void Behaviour:** void fractions downstream of the HX decreased as the flow moved through the downcomer and horizontal pipe sections toward the heater. Conversely, void fractions increased as flow moved upward in the riser after the heater, highlighting the role of hydrostatic pressure in condensation and boiling processes.

- **Pipe Orientation and Interfacial Area:** the orientation of pipes (vertical vs. horizontal) significantly influenced the size of the interfacial area between steam and liquid, thereby affecting condensation rates. This highlights the importance of considering pipe orientation when analysing density variations and their impact on flow behaviour.
- **Insulation and Heat Losses:** considering the fluctuating phenomena occurring within the loop, not only in the heater and the HX, despite the model is assumed fully adiabatic, highlights the importance of ensuring proper insulation and heat loss management in the planned facility.

These phenomena suggest that interfacial friction between steam and liquid is a critical parameter requiring further sensitivity analysis to the interfacial correlation adopted by the system codes. Such analysis would provide a more accurate assessment of the system code's predictive capabilities and enhance the understanding of flow dynamics within the loop.

The Role of User Effect and Code Comparison

The user effect was observed when comparing simulation results between Apros and C-3. Differences in user-defined configurations and methodologies demonstrated the need for a standardized code-to-code comparison protocol. Such a protocol would ensure consistency, avoid resource wastage, and reduce the risk of generating inaccurate data.

Facility-Specific Considerations

For the ALCINA facility, the analysis highlighted the importance of precise parameter measurement sensors and robust insulation. Temperature variations within the loop were found to significantly affect flow behaviour. Minimizing heat losses will be essential to achieve accurate analysis and predictions, especially for natural circulation studies.

Addressing Uncertainties and Limitations

The uncertainties associated with this exercise are significantly high, but the primary objective was to gain insights into natural circulation phenomena rather than validate the code. Further investigation into system codes is necessary, particularly regarding the role of damping terms, as current findings suggest that system codes may artificially reduce damping. Determining whether this phenomenon is physical or purely numerical remains a key area for future research.

Conclusion and Recommendations

This analysis successfully advanced the understanding of natural circulation phenomena in closed-loop systems. However, several recommendations for future work emerged:

1. To perform sensitivity analyses on interfacial friction correlations to better assess system code capabilities.
2. To test and refine control logic configurations to reduce non-physical flow fluctuations.
3. To Incorporate comprehensive measurement devices and robust insulation in the planned experimental facilities to confirm phenomena and to manage heat losses through proper insulations.
4. To develop a standardized protocol for code-to-code comparisons to streamline methodologies and ensure consistency.

5. To investigate the role of hydrostatic pressure, pipe orientation, and void behaviour in condensation and boiling processes.

By addressing these areas, future studies can reduce uncertainties, enhance system code validation and comparison, and improve the accuracy of predictions for natural circulation phenomena in experimental setups.

5. Summary

This report shows the simulation conducted for 200 two-phase cases, with two rounds, conducted using Apros with two heat exchanger (HX) geometries: a 250 mm and a 400 mm HX. The results consistently showed overestimation of mass flow rate and void generation, along with underestimation of outlet temperature. In the 400 mm HX, some cases deviated by underestimating flow rate. The simulations neglected the APSARA facility's constraint of pure liquid flow from the steam drum outlet to focus on evaluating HX length and associated phenomena.

A user-defined convergence criterion requiring inlet temperature variation within ±0.5 °C was applied to identify cases with minimal fluctuations. Differentiating physical fluctuations from numerical ones was challenging, particularly as control logic fluctuations and pressure drops caused instability. Feedwater control logic, adjusted based on temperature after the HX, contributed to simulated flow fluctuation, due to rapid controller responses leading to significant pressure drops. These findings underscore the importance of stable input locations and robust control logic configurations.

The study highlighted several flow phenomena. Void fractions decreased downstream of the HX but increased after the heater due to hydrostatic pressure effects. Pipe orientation significantly influenced interfacial area size, affecting condensation rates and density variations. Additionally, despite the adiabatic assumption, heat loss management and proper insulation were identified as critical for accurate analysis.

A comparison between Apros and C-3 simulations revealed differences, yet both showed acceptable agreement and overall behaviour. The user effect is a crucial factor in code-to- code comparison exercises, emphasizing the need for a standardized code-to-code comparison protocol to ensure consistent methodology.

For the ALCINA facility, robust insulation and precise measurement sensors were identified essential to enhance analysis accuracy. The study revealed high uncertainties, highlighting the need for further investigation into interfacial friction correlations, hydrostatic pressure effects, and the role of damping terms. These efforts will improve system code validation and understanding of natural circulation in closed-loop systems.

6. References

[1] G. R. D. P. P. V. a. D. S. P. Dubey, “ANALYSIS OF EXPERIMENTAL DATA ON TWO-PHASE NATURAL CIRCULATION FROM THE FLOW PATTERN TRANSITION INSTABILITY STUDIES FACILITY AT APSARA REACTOR,” Bhabha Atomic Research Centre, Mumbai, 2004.

[2] B. A. R. Center, “50 Glorios Years of APSARA,” Bhabha Atomic Research Center , Nunbai, 2007.

[3] F. Alblouwy, “Analysis of APSARA Test Facility Data with Apros and CATHARE-3 Codes,” SAFER2028-VTT, Espoo, 2024.

[4] “13. Pipe Drawings,” OpenOregon Educational Resources, [Online]. Available: https://openoregon.pressbooks.pub/weldsymbols/chapter/pipe-drawings-2/.

[5] I. Idel'chik, HANDBOOK OF HYDRAULIC RESISTANCE, U.S. Atomic Energy Comisison, 1966.

[6] “Apros-Product Information,” [Online]. Available: https://www.apros.fi/product-information/brochures/.

[7] “CATHARE Thermal-Hydraulic Simulation of Multiphase Flow Dynamics,” CEA, [Online]. Available: https://cathare.cea.fr/.

[8] P. G. Y. L. Solomon Bello, “Closed-loop experimental investigation of single-phase natural circulation flow phenomena based on temperature and heating power variations,” *Annals of Nuclear Energy,* p. 10, 2021.

[9] F. M. White, Fluid Mechanics (7th Edition), Mc Graw Hill.

[10] “Python Numerical Methods,” [Online]. Available: https://pythonnumericalmethods.studentorg.berkeley.edu/notebooks/chapter24.03-Fast-Fourier-Transform.html.

[11] L. D. S. S. a. B. S. Klaus Umminger, “Integral Test Facility PKL: Experimental PWR,” *Science and Technology of Nuclear Installations,* 2011.

[12] Framatome, “Framatome.com,” [Online]. Available: https://www.framatome.com/EN/customer-819/pkl-pwr-integral-system-test-facility.html. [Accessed 02 2022].

[13] Y. X. Z. Z. Xiande Fang, “New correlations of single-phase friction factor for turbulent pipe flow and evaluation of existing single-phase friction factor correlations,” *Nuclear Engineering and Design,* p. 6, 2010.

[14] A. K. N. a. N. K. Pallippattu Krishnan Vijayan, Single-Phase, Two-Phase and Supercritical Natural Circulation Systems, 2019.

[15] I. A. P. K. M. J. N. B. V. G. Srbislav Genić, “A Review of Explicit Approximations of Colebrook’s Equation,” 2011.

[16] Y. X. Z. Z. Xiande Fang, “New correlations of single-phase friction factor for turbulent pipe flow and evaluation of existing single-phase friction factor correlations,” *Nuclear Engineering and Design,* p. 6, 2011.

[17] “Apros Refernce Manuals,” VTT Technical Research Centre of Finland (VTT), 2019.

[18] R. B. D. T. J. D. Igor L. Pioro, “Hydraulic resistance of fluids flowing in channels,” *Nuclear Engineering and Design at supercritical pressures (survey),* p. 11, 2004.